Electronic Theses and Dissertations         Theses, Dissertations, and Major Papers

7-11-2015

# Improved Internal Relief Valve Performance Through Study Of Reduced Cracking To Full By-Pass Pressure Using CFD Simulation

Yohance Bakari Henry
*University of Windsor*

Follow this and additional works at: https://scholar.uwindsor.ca/etd

# IMPROVED INTERNAL RELIEF VALVE PERFORMANCE THROUGH STUDY OF REDUCED CRACKING TO FULL BY-PASS PRESSURE USING CFD SIMULATION

By

YOHANCE HENRY, M.Eng., P.Eng.

A Thesis
Submitted to the Faculty of Graduate Studies
through the Department of Mechanical, Automotive & Materials Engineering
in Partial Fulfillment of the Requirements for
the Degree of Master of Applied Science
at the University of Windsor

Windsor, Ontario, Canada

2015

© 2015 Yohance Henry

# IMPROVED INTERNAL RELIEF VALVE PERFORMANCE THROUGH STUDY OF REDUCED CRACKING TO FULL BY-PASS PRESSURE USING CFD SIMULATION

by

**Yohance Henry, M.Eng., P.Eng.**

APPROVED BY:


_____
Dr. N. Biswas
Department of Civil and Environmental Engineering


_____
Dr. G.W. Rankin
Department of Mechanical, Automotive and Materials Engineering


_____
Dr. R.M. Barron, Co-Advisor
Department of Mechanical,
Automotive and Materials Engineering

_____
Dr. R. Balachandar, Co-Advisor
Department of Mechanical,
Automotive and Materials Engineering

May 19th, 2015

# DECLARATION OF ORIGINALITY

I hereby certify that I am the sole author of this thesis and that no part of this thesis has been published or submitted for publication.

I certify that, to the best of my knowledge, my thesis does not infringe upon anyone's copyright nor violate any proprietary rights and that any ideas, techniques, quotations, or any other material from the work of other people included in my thesis, published or otherwise, are fully acknowledged in accordance with the standard referencing practices. Furthermore, to the extent that I have included copyrighted material that surpasses the bounds of fair dealing within the meaning of the Canada Copyright Act, I certify that I have obtained a written permission from the copyright owner(s) to include such material(s) in my thesis and have included copies of such copyright clearances in my appendix.

I declare that this is a true copy of my thesis, including any final revisions, as approved by my thesis committee and the Graduate Studies office, and that this thesis has not been submitted for a higher degree to any other University or Institution.

# ABSTRACT

Relief valves are widely used in the process industry. Their ultimate role is to mitigate adverse conditions that would jeopardize safety and incur catastrophic losses, especially with respect to human life. The primary focus of this research is to investigate the performance of relief valves, with the specific objective of reducing the cracking to full by-pass pressure in internal relief valves of positive displacement pumps. Two and three-dimensional computational fluid dynamics (CFD) models of an external relief valve are developed and used to evaluate the effects of the mesh, numerical parameters and boundary conditions on the results, including flow pressure and velocity field. Knowledge gained from the external relief valve study has guided the internal relief valve simulations, particularly with regards to sensitivity of the results to the mesh and other numerical settings. Numerical simulations were performed utilizing the CFD codes: ANSYS Fluent and STAR-CCM+.

# DEDICATION

To my wife Keisha Henry and our three wonderful boys

Yohance Jr., Djimon and Ajani Henry

also

To my parents, Gordon and Erma Henry,

and my sister, Mariama Henry.

# ACKNOWLEDGEMENTS

# TABLE OF CONTENTS

# LIST OF TABLES

# LIST OF FIGURES

# LIST OF APPENDICES

## APPENDIX A - Copyright Permission Documents

## APPENDIX  B - Calculations

# LIST OF ABBRREVIATIONS/SYMBOLS

| | |
|---|---|
| ACSL | Advanced Continuous Simulation Language |
| API | American Petroleum Institute |
| ASME | American Society of Mechanical Engineers |
| CFD | Computational fluid dynamics |
| CPRV | Charge pressure relief valve |
| ERV | External relief valve |
| IRV | Internal relief valve |
| PMMA | Polymethyl methacrylate |
| NPSHa | Net positive suction head available |
| NPSHr | Net positive suction head required |
| NSE | Navier-Stokes equation |
| SLSV | Spring-loaded safety valves |

# NOMENCLATURE

| | |
|---|---|
| $k$ | Kinetic energy of turbulence |
| $\varepsilon$ | Dissipation rate of turbulence |
| $\omega$ | Dissipation rate of turbulence (turbulent frequency) |
| $C_b$ | Correction coefficient |
| $C_D$ | Drag coefficient |
| $C_d$ | Discharge coefficient |
| $C_v$ | Velocity coefficient |

# CHAPTER 1. INTRODUCTION

Internal relief valves (IRV) are mounted as over-pressure protection devices on internal gear pumps. The IRV's main role is to reduce the pressure if an over-pressure situation occurs. The IRV can be viewed as a robust safety feature, but most internal/external gear pumps do not have them as part of a standard design. This is due to a combination of cost and design criteria needed to implement the IRV on the gear pump. Very little research has been done towards improving the IRV's performance. The IRV design specifically related to Viking Pump Inc. has been in existence for over 100 years with very little change to the design. The major hurdles with researching these components are mainly the accessibility in viewing the flow pattern and understanding how the flow pattern changes if components are modified within the IRV.

Internal gear pumps are a positive displacement pump, which means that the discharge head vs. flow characteristic is vertical, thus the flow is inherently independent of the discharge head. Liquid is rotated from suction to discharge through cavities within the gear teeth and casing. If there is a blockage on the discharge side of the pump, such as a valve being closed in the discharge line, there will be an immediate pressure build-up. This pressure build-up could be catastrophic if it is not mitigated immediately or at least within a suitable time. If this occurs, the pump will fail internally, or the motor will stall, or the drive equipment will fail, or the process piping will fail catastrophically. It is because of these potential failures and the severe consequences that it is imperative that some form of over-pressure protection be used in internal gear pump arrangements. This protection could be through the use of an internal relief valve, an external relief valve, a torque limiting device or a rupture disc.

There is great interest in improving the relief valve performance of internal gear pumps. There are many key advantages related to internal gear pumps that could be gained from research carried out towards improving the IRV performance. These improvements could help pump companies be more competitive from an applications standpoint by reducing the customers' operating costs while improving safety. A detailed understanding of the liquid flow inside the IRV will also help to design more efficient internal gear pumps for applications involving thin liquids operating at high pressures. Further details with regard to potential improvements will be discussed later in this thesis.

The internal relief valve is composed of three main components, the poppet, spring and adjusting screw. These three components are essential for setting the cracking pressure (pressure at which the IRV begins to open) at which the poppet begins to lift, forming an orifice with the seat while pushing against the spring to create full by-pass in an over-pressure situation. The concepts behind this full operation will be highlighted and explained later in this thesis.

A preliminary computational fluid dynamics (CFD) study was first performed on a simple model of an external RV, primarily to get a feel for the main characteristics of the flow fields associated with RVs, such as: the pressure field, velocity field, regions of separation and flow streamlines. This exercise included preliminary validation of the numerical models and the opportunity to become more familiar with the software and how results are affected by different parameter settings. Based on the experiences gained in the preliminary study, a CFD model of a Viking Pump Inc. IRV has been set up and analyzed at the fully open condition.

The main goals/motivation of this thesis are:

1. to understand how CFD can be leveraged, in lieu of the availability of physical hardware and instrumentation typically reserved for laboratory research simulations;

2. to optimize the parameters that favour a reduced range of cracking to full by-pass pressure in internal and external relief valves and therefore improve their performance. The pump is sized at the differential pressure. The cracking pressure is equivalent to the differential pressure.

# CHAPTER 2.   LITERATURE REVIEW

## 2.1.    Introduction

Several journal articles, papers and reports produced by valve companies were reviewed to evaluate the performance status of relief valves. No research exists with respect to internal relief valves. The following review of the available literature, however, highlights those results which offer some guidance and reflections on the goals of this thesis.

## 2.2.    Previous Studies Related to Internal/External Relief Valves

Mayer et al. [1] conducted a study to obtain information on the operation of  the Viking Pump IRV. The main characteristics studied involved flow vs. pressure as well as poppet lift (calculated and measured). The information obtained from the study was used to develop the governing mathematical equations and a FORTRAN computer program to model the flow through internal relief valves.

The steady-state flow force equation, spring force and drag force on poppet were used in the force analysis of the poppet. Drag coefficient ($C_D$), discharge coefficient ($C_d$) and velocity coefficient ($C_v$) were determined from performance tests and poppet lift measurements. From this analysis, the equation and computer program that was used to determine the flow area for a given poppet lift, poppet seat angle and poppet diameter was highlighted. Graphical relationships of poppet lift (measured and calculated) and capacity vs. discharge were developed to predict relief valve performance at various viscosity values.

For specific relief valves in operation while the pump was running at speeds in the 500 RPM to 1200 RPM range, it was noted that the calculated and measured poppet lift exhibited the same approximate relationship. These findings were documented in Viking's Pump Internal Archive W.O. 4592 [1].

Kourakos et al. [2] investigated the external relief valve (ERV). The main focus of their investigation was to determine the forces imposed on the valve disc for different inlet pressures and different disc positions using both experimental and CFD results. They used a 40 mm (1.5 in.) ERV for the experimental setup. The ERV was modified by removing the spring. A force measuring device was mounted on top of the valve. With this experimental setup, they determined the forces applied on the disc at different inlet pressures and disc positions. For each iteration, the disc was set at a new lift position (static position). Chosen set pressures and valve lift from preliminary dynamic valve operation investigations were provided to analyze the forces imposed on the disc.

The experimental apparatus consisted of two ERV models, viz. a metallic model and a transparent model made of polymethyl methacrylate (PMMA), with slight design differences. The metallic ERV model was used to analyze incompressible flow while the transparent model was used to analyze compressible flow. One notable difference between the two models is that the plastic model had a longer inlet nozzle when compared to the actual metallic ERV. Another important difference was the ability for the original metallic ERV to handle higher pressures. The differences between these valves can be observed in Fig. 2.1.
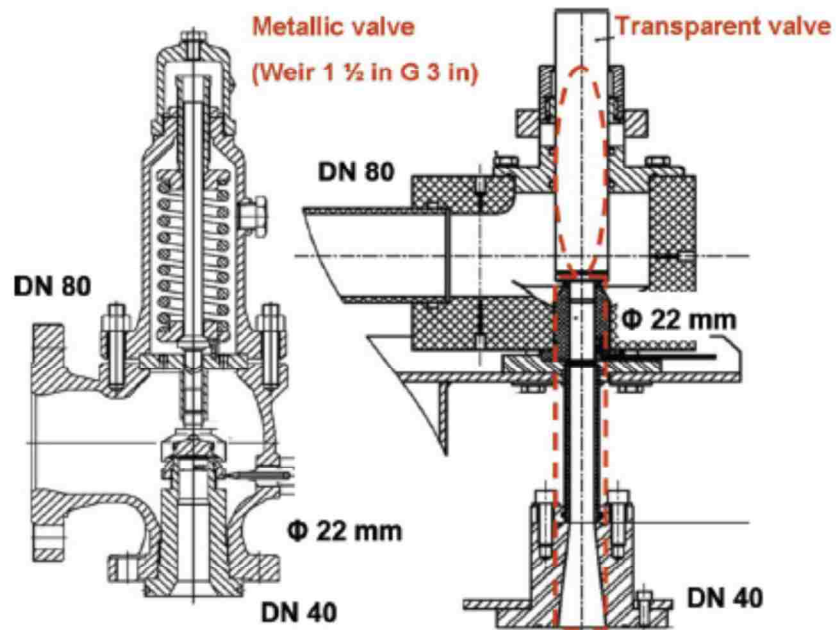
Fig. 2.1: Comparison of metallic and transparent valves

(from Kourakos et al. [2], by permission of ASME)

Having a transparent valve allowed for complete optical visualization and observation of the flow through the valve as well as cavitation and two-phase flow. Kourakos et al. [2] studied these effects in compressible and incompressible environments. Further highlights of how Kourakos et al. [2] analyzed the transparent and metallic valves are shown in Fig. 2.2 and Fig. 2.3.
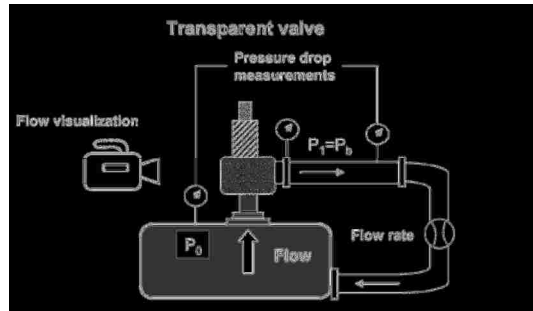
Fig. 2.2: Transparent valve used by Kourakos et al. [2]

(by permission of ASME)
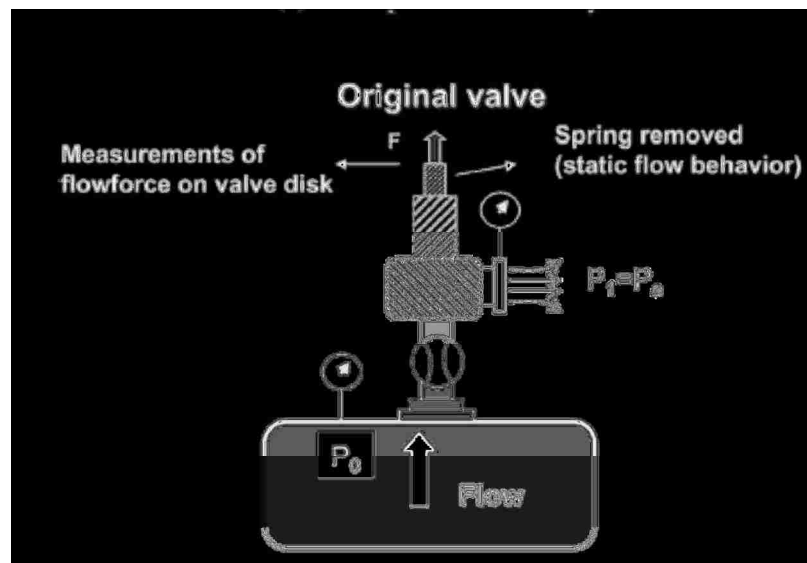


Fig. 2.3: Metallic valve used by Kourakos et al. [2]

(by permission of ASME)

In the experimental setup involving the metallic valve, the back pressure affects how the valve disc behaves. In the transparent model several pressure sensors were placed inside the valve. These allow for measurements of static pressure. In addition to measuring pressure inside the valve, additional pressure sensors were placed directly on the valve disc to obtain information on the disc flow force. As stated above, the metallic

model is able to handle higher pressures compared to the transparent model. However, there is limited optical access with the metallic model and only the set pressure and back pressure can be measured with this model.

Since our interest in the current research is to study the flow of water through a RV, only the incompressible environment of Kourakos et al. [2] will be discussed further. In the experimental setup shown in Fig. 2.4, the metallic ERV is analyzed using water at ambient temperature as the test fluid. The calming reservoir is connected to a pump capable of producing pressure up to 78 bars (1146 psi) and 250 $m^3$/hr (1101 gpm) flow rate. The admission valve acts like a variable frequency drive (VFD) to control the flow entering the calming reservoir which leads to the long pipe connected to the test ERV. The admission valve admits a certain percentage of flow into the calming reservoir. The author suggest that this is analogous to a variable frequency drive as it also acts as a flow control device by reducing the motor speed of the pump which will only allow a certain percentage of the flow to leave the pump going into the process. Pressure on the free surface of the reservoir is fixed by compressed air. The flow rate entering the ERV is measured by a flow meter. To obtain the best efficiency of the pump, the discharge valve operates as a by-pass. This setup permits the observation of opening pressure, closing pressure and the discharge coefficient. Also, the approximate flow force on the disc is acquired as well with sensors mounted on top of the valve. The flow conditions analyzed in the ERV test setup are Pset = 0.7 - 11.0 bar (10.2-160 psi) and lift values at 0.5 to 7.2 mm (0.02 to 0.283 in.)

Computational Fluid Dynamics (CFD) simulations of the test ERV were also performed in [2] using ANSYS Fluent [version 13]. A simplified geometry was created

for the simulations, with a 2D axisymmetric grid as shown in Fig. 2.4. The grid, which

contained $1.45 \times 10^6$ cells, was designed with a particular focus on the disc region since

the primary interest was to determine the flow force on the disc. A steady-state case was

assumed and the $k$-$\omega$ turbulence model was used with a second order discretization

scheme. The pressure based solver of Fluent (pressure-velocity coupling) was used. The

following set pressures and lift values were analyzed with the CFD model: Pset = 2, 3, 6

and 11 bar (29, 43.5, 87 and 159.5 psi) and lift values at 1.5, 3, 4.5 and 7.2 mm (0.06,

0.12, 0.18, 0.28 in.)
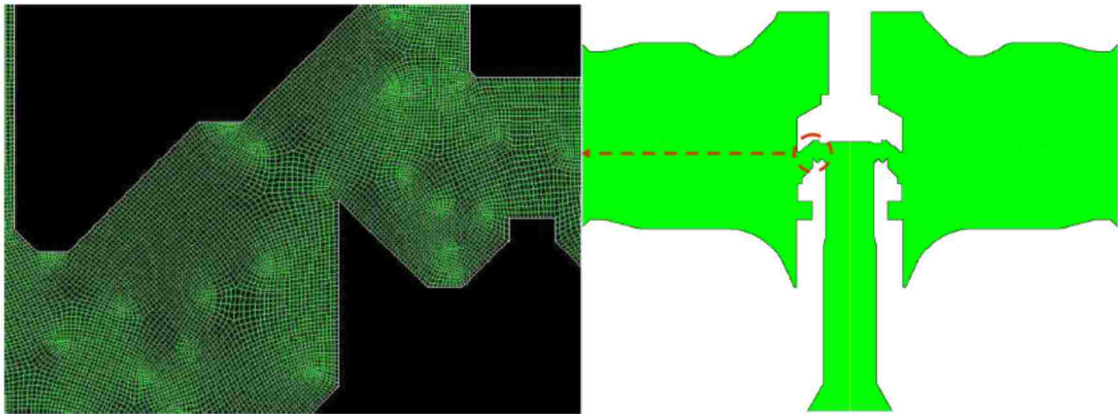


Fig. 2.4: Axisymmetric grid for the metallic ERV [2]

(by permission of ASME)

To simplify the problem and to decrease computational time, the incompressible

flow was assumed to be steady and cavitation was neglected. From the CFD results,

Kourakos et al. [2]  concluded that the lowest lift produced the highest pressure

concentration in the middle of the disc, whereas higher disk lift positions produced a

more uniformly distributed pressure over the valve disc. Due to these phenomena, the

force gradient is more severe for lower disc lifts compared to higher lifts. When

experimental and CFD results are compared, the measured and CFD computations provide reasonable predictions in flow force with CFD computations. Small deviations existed between the tested and computational values. The adjustment ring location for the experiment created some experimental uncertainty.

The research conducted by Chabane et al. [3] concentrates on ERV's subjected to back pressure build up. They indicate that real world safety relief valves, having a back pressure that is 30% of the set pressure, generally use a balancing mechanism called a bellows. The bellows helps to facilitate the reduction of the forces downstream, resulting in the balancing out of the downstream pressure. This helps to avoid vibration/chatter usually caused by back pressure. A poorly designed ERV can prove disastrous if back pressure values are high. It is stated that a conventional ERV at 10% of the set pressure can be used without the balancing effects, however even with low values of back pressure fluttering/chattering of the disc may still occur. Comparing the conventional ERV to the balanced bellows ERV, the balanced bellows ERV should be able to handle levels of back pressure in the vicinity of 40 - 50% of the set pressure, while maintaining its approximate capacity.

Chabane et al. [3] looked at the ERV and the effects of back pressure from a theoretical perspective. In theory, correction factors for back pressure can be obtained from the American Petroleum Institute (API) - API 520 Code. The code presents the correction coefficient ($C_b$) for back pressure values obtained from numerous ERV tests and use an average value for $C_b$ for a particular case. They noticed one major flaw in the analysis – that these coefficients do not take into account the instabilities due to dynamic

effects caused by back pressure. According to the API 520 Code, experiments have shown that instabilities could occur with as little as 15% back pressure.

An experiment to evaluate this concept further was setup by Chabane et al. [3] using air with the ERV pressure set at 40 bar (580 psi). The air in the downstream reservoir was at 200 bar (2900 psi). Flow rates were measured using four Coriolis flow meters. The flow meters were linked to a buffer tank where the ERVs were tested. Maximum pressure attainable was 40 bar (580 psi) and maximum mass flow rate was 13 kg/s (29 lb/s). The effects of pressure are detected when back pressure rises to about 10% of set pressure. When back pressure is higher, characteristics of the air flow change. Vibration and chattering occur when back pressure reaches values that are 25% to 30% of set pressure.

A CFD model was also developed by Chabane et al. [3] for the numerical simulation of the ERV and was validated with the experimental data. The CFX-11 code was used to solve the 3D Reynolds-Averaged Navier-Stokes equations. No symmetric considerations were assumed. A 3D unstructured mesh was used, comprised of 15,500,000 cells (3,000,000 nodes). Tetrahedral/prismatic elements were used close to the wall, at the nozzle and disc valve to ensure a Y+ value below 100. Unstructured tetrahedral elements were used away from the walls. A steady flow approach was assumed, using the $k$-$\varepsilon$ turbulence model with wall functions and $2^{nd}$-order discretization accuracy. Three cases were analyzed and compared to the experimental results; Case 1: disc in almost closed position. Case 2: disc ½ way closed, and Case 3: disc at fully open position. Analysis of the flow patterns in these three cases confirms that the dynamics of the flow are complex due to the moving disc. At full flow (Case 3) there is significant

11

turbulence which causes load fluctuations. These fluctuations influence the movement of the blocking area (disc). Fluctuations also occur at lower disc lift. Due to stiffness of the valve at smaller openings, the hydrodynamic forces vary between two and three times the value of the elastic force associated with the spring.

A thermodynamic model with test conditions was also developed by Chabane et al. [3]. Due to compressibility of the air and gas the fast unsteady effects are normally considered insignificant and are not taken into account. Since there is a possibility that equilibrium cannot reached due to pipe and control valve downstream creating back pressure, this could lead to chattering, which can be destructive to the safety valve depending on its frequency. This model was implemented to better understand the dynamic behaviour during a test with and without back pressure. Equations of motion were developed to help understand these effects.

It was important to get an idea of how back pressure affects the ERV when at a certain percentage of the set pressure. In this Thesis the assumption is made that back pressure effects are accounted for in the calculation of the differential pressure. The pump is sized at the differential pressure before the IRV setting is applied.

Follmer and Schnettler [4] proposed developing a series of new API ERVs by investigating the fluid flow and looking into a new method to perform flow force measurements. They were able to analyze which components in contact with liquid could be removed or improved. This was done to implement a series of new API ERVs which could meet industry certification standards.

With regards to approval testing, only combinations of flow force and spring force were checked in accordance with API 526 designation, which is a specific method

of measurement for flow force by API 526 Codes. This method permits the accurate evaluation of flow force readings over a large pressure range. Thus, forces on the disc can be evaluated from the flow force for various opening and closing values. The following conditions have to be met. The interaction between flow force and spring force is essential. This will help to determine what type of spring characteristics are needed. Also the flow coefficient needs to be large enough to stay within the +/-5% tolerance band while maintaining its consistency (constant) while subjected to a pressure of 1 bar (14.5 psi) and up.

Optimization of the components was carried out using gases, steam and liquids. The blow down ring was removed as it does not impact the flow physically. The blow down ring is a component which controls how slowly and how fast the disc closes. The term blowdown defines the disc moving down to close. The position of the blowdown ring will determine how slow or how fast the disc closes. Calculations (CFD) were performed for 3D compressible and incompressible flows. Based on the CFD analysis, which was confirmed experimentally, a special ERV was designed that provided a proportional performance and consistent opening for 100 bar (1450 psi) pressure and hot water at 265°C. This valve was designed to conform to all API 526 specifications along with approvals by ASME. The valve also was improved and optimised to accommodate equal flow geometry for liquids (incompressible), gases and steams and also incorporates the ability to handle two-phase flows if needed.

Bilanin and Teske [5] investigated spring-loaded safety ERVs. Their goal was to try to predict the performance of the ERVs numerically. They used the concept of a semi-empirical non-linear model of a safety ERV and were able to derive dynamic equations

from this model. Bilanin and Teske [5] implemented this model and developed the COUPLE predictive dynamic model to simulate flow through an ERV. The COUPLE model was used to explain the test data of the ERV such as chatter, lift characteristics, etc. The COUPLE code incorporated the flow path of the valve by specifying spring rate and the ring settings. The valve models were validated through experiments.

Using CFD, the Navier-Stokes equations (NSE) were also used by Bilanin and Teske [5] to predict the flow field within the valve. The governing differential equations used to model the flow field were the Reynolds-Averaged Navier-Stokes equations. A comparison of the Navier-Stokes solution and the predictions from the COUPLE code was performed. The NSE results replaced the experimental testing for validation purposes with respect to the COUPLE code. Exit angle, mass flow through the valve, seat force reduction and stem force on lifted ERVs were compared at different valve stem positions.

Oravec [6] investigated pressure rise rate characteristics and flow force acting on a poppet in a charge pressure relief (CPRV). They are both direct acting poppet style relief valves, where in an over pressure situation the poppet is lifted and allows flow to recirculate through the relief valve and back to the process or through the pump. The operation of the charge pressure relief valve is very similar to the internal relief valve. However, it can also be used in the process line, unlike the IRV which can only be used directly on the pump. The CPRV was analyzed using CFD and subsequently verified with experimentation. Three stroke positions were considered with poppet lift values of 0.5 mm, 1.5 mm and 3 mm, while being subjected to a range of flow rates. ANSYS ICEM CFD was used with a combination of a hexahedral, tetrahedral and wedge mesh. Velocity inlet and pressure outlet boundary conditions were established, the flow was assumed to

be steady and the fluid was taken to be incompressible (oil). Post-processing of the CFD results was completed using three strokes (lift values) and three flow rates. From this data, a quadratic equation was used to solve for flow rate, highlighting the relationship between spring force and flow force. Graphs were generated from calculated points and trend lines were implemented to support the data points.

For validation purposes, an experimental setup of the CPRV was prepared. It is important to note that neither the CFD nor the experimental setup incorporated the dynamic aspects. The CFD simulation was compared to the experimental simulation using flow rate and pressure drop across the CPRV [6].

Pressure vessels normally have spring-loaded safety valves (SLSV) in the event of an over-pressure situation. Sethi and Lai [7] explored the dynamic behaviour of SLSVs. Generally, the forces acting on the moving parts of these valves are non-linear. A differential equation model was developed to simulate the non-linear effects of the SLSV. This model was used to predict the valve response time. In solving these equations, the Advanced Continuous Simulation Language (ACSL) was used to facilitate solution of the 4$^{th}$-order differential equations utilizing the Runge-Kutta method. Sample tests of the Farris 7000 valve were conducted to acquire pressure time history. The response to the valve, related to the driving pressure, was illustrated graphically and compared to the simulated study. There was close agreement between the simulated and experimental data. In conclusion, the simulated results seemed to predict the actual results fairly well.

The articles reviewed above are mainly associated with the ERV. There is not much published literature on the IRV. One main difference between the IRV and ERV is that the IRV spring is always in contact with fluid during by-pass. This is not the case

15

with the ERV. However, the flow fields are in general very similar and the operation in an over-pressure situation is identical when comparing the ERV to IRV. The similarity of these concepts suggests a close relationship between the physics associated with ERVs and IRVs which has been exploited in this thesis.

The major research motivation in this thesis is to reduce the cracking to full by pass pressure in the IRV. A more in depth discussion regarding research motivation will be discussed in Chapter 5.

# CHAPTER 3. INTERNAL GEAR PUMP AND RELIEF VALVE OPERATION

It is essential to understand the internal gear pump operation and how it relates to relief valve operation. The pump operation is explained in this chapter, followed by a focus on the specifics behind the internal and external relief valve operation.

## 3.1. Internal Gear Pump Operation

The internal gear pump operates on a fairly simple concept. The term "positive displacement" is a direct representation of how internal gear pumps operate. Referring to Fig. 3.1, at Step 1 the liquid enters the rotor and idler gear as the pump develops pressure. The arrows indicate the direction of the flow. At Step 2 the liquid travels between the teeth of the rotor and idler gear teeth separately (gear within a gear principle). The moon shaped crescent helps to divide the liquid and acts as a seal between the suction and discharge ports. At Step 3 the pump is nearly flooded and the gear teeth have a finite volume of fluid between them. In Step 4 the rotor and idler teeth are completely aligned to form a seal. As the liquid now has nowhere else to go, it is forced out of the port into the discharge process line.
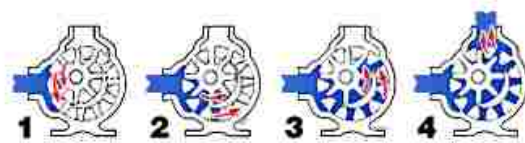


Fig. 3.1: Internal gear pump operation

(from http://www.vikingpump.com [8], by permission of Viking Pump Inc.)

## 3.2. Internal Relief Valve Operation

The IRV is the most important component on internal gear pumps with regards to safety. It is directly mounted on the pump and is the sole device that provides protection against over-pressure inside the pump. Figure 3.2 illustrates an IRV mounted on an internal gear pump.



Fig. 3.2: Internal gear pump with IRV mounted on top

(from http://www.vikingpump.com [8], by permission of Viking Pump Inc.)

When an over-pressure situation occurs, the IRV allows the fluid to recirculate inside the pump until the pressure is brought down below the setpressure point. The mechanism by which this occurs can be explained by referencing Fig. 3.3. The spring (A) holds the poppet in place. The poppet guide vanes rest on the internal wall of the IRV in the valve body (C), while the spring (A) holds the poppet (B) against the valve seat. This position of the poppet is maintained by a force which is determined by the spring size as well as how tightly the spring is compressed by the adjusting screw (D). In an over-pressure situation, the pump discharge pressure pushes against point (E) on the poppet. When this occurs, the force exerted by the liquid under the poppet exceeds the force

exerted by the spring (set force or set pressure of the spring) and the poppet begins to lift. When the poppet lifts the liquid begins to flow through the IRV and return back into the suction port of the pump. As the pressure keeps building up past the set pressure, all the liquid will eventually flow through the valve and back into the pump. At this point no liquid will be leaving through pump discharge. This recirculation will continue until the force or pressure drops below the set force or pressure value at which the spring was originally set.
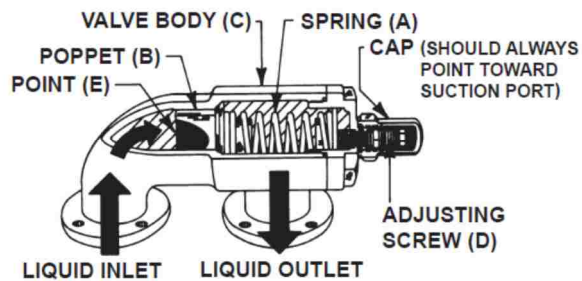


Fig. 3.3: Cutaway of Viking internal pressure relief valve [9]

(by permission of Viking Pump Inc.)

## 3.3. External Relief Valve Operation

The ERV operates on exactly the same concept as the IRV with regards to the spring set pressure. Figure 3.4 illustrates a typical ERV. The IRV and ERV have very similar flow fields.
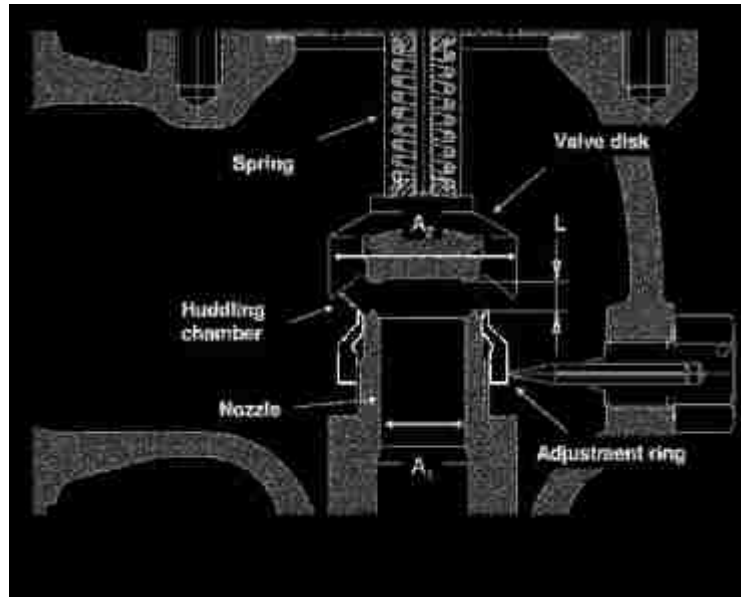
Fig. 3.4: Detailed view of nozzle and valve disc [2]

(by permission of ASME)

The ERV operates on exactly the same principle as the IRV. When the spring force is overcome by the force of the liquid coming through the nozzle, the spring compresses and the valve disc opens. The valve disc will not close until the force of the liquid drops below the spring force (set pressure of spring). It can be noted as well that the cross-sectional area of the valve disc ($A_2$) is designed to be larger than that of the nozzle ($A_1$). For a constant system pressure, when the fluid exits the nozzle and enters a larger area the disc will experience a larger force that will prevail over the disc and thus the spring force keeping the disc open. This could result in the valve subsequently opening too quickly. Flow velocity could cause changes in valve lift by changing the lift height. Due to this larger area, the valve disc will not close until the system pressure goes below a certain value (percentage) of the set pressure, referred to as the blow down pressure. The huddling chamber is located between the nozzle exit and disc as illustrated

20

in Fig. 3.4. Its geometry is one of the factors determining when the valve will close. The adjustment ring is used to control the opening or re-seating characteristics of the disc. The adjustment ring is installed on the nozzle and can be found on most ERVs, but not all ERVs are equipped with this feature.

# CHAPTER 4.   CFD SIMULATION OF AN EXTERNAL RELIEF VALVE

## 4.1.      Introduction

As mentioned above, the external relief valve (ERV) exhibits flow features that are similar to the internal relief valve (IRV), but the geometry of the ERV flow region is simpler than the IRV. In this research the ERV was used as a starting point to investigate meshing requirements, numerical parameter settings in the software and key features of the flow field. Gambit and ANSYS Fluent [version 13] Computational Fluid Dynamics (CFD) software were used for mesh generation and to perform the CFD simulations, respectively. A simplified ERV design was used to reduce difficulties associated with generation of the mesh. Both two-dimensional (2D) and three-dimensional (3D) ERV simulations were carried out.

## 4.2.      External Relief Valve (2D simulation)

A simplified 2D model of an external relief valve was utilized for the first stage of the CFD study. The simplified ERV model was developed by using a typical ERV as a reference, as shown in Fig. 4.1. The circled area of the ERV in Fig. 4.1 was used to represent the key geometric features retained in the preliminary model.
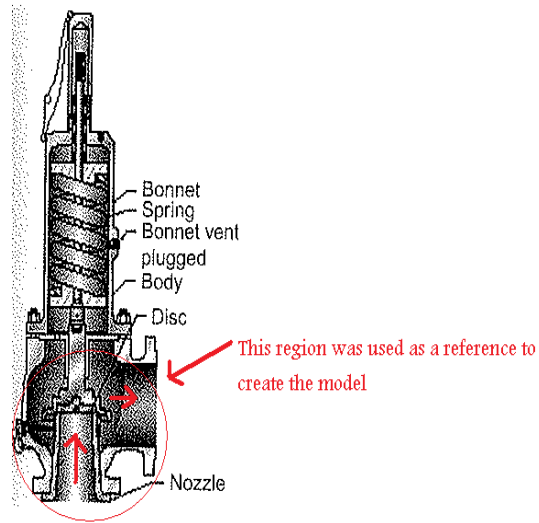
Fig. 4.1: General design of a spring operated safety relief valve

(from Helleman [10], by permission of Elsevier)

The objective of this exercise was to model a flow field similar to, but less complicated than the IRV. In doing so, the simplified 2D model of the ERV was used to determine appropriate settings that should be used for the 3D simulations of the ERV and IRV. The simplified ERV analysis provides the necessary knowledge and tools needed to entertain the more complicated IRV design, which is the main focus of this thesis. Settings of particular interest are:

- turbulence model;

- type of upwinding, i.e., $1^{st}$ or $2^{nd}$-order to achieve greater theoretical accuracy;

- the convergence criteria, which can be manipulated with a tighter tolerance band to achieve better results;

- relaxation factors, which can be adjusted to help smooth out the oscillations of residuals and accelerate convergence, based on a specific convergence criteria.

With respect to the ERV model, certain assumptions were made to simplify the geometry and for the computational analysis. The ERV was initially modelled with a simplified rectangular design as shown in Fig. 4.2. The diameters of the inlet and outlet were assumed to be the same. This was done to simulate the IRV, where the inlet and outlet ports are the same size. The outlet was taken flush with the side wall.

The mesh employed for the ERV simulation was a structured quadrilateral mesh as shown in Fig. 4.2. Clustering was applied along the solid walls and at sharp corners to capture boundary-layer effects and regions of flow separation. Cell aspect ratios ranged from 1.0 and 1.04.



Fig. 4.2: Clustered mesh with boundary conditions

An incompressible Newtonian fluid (water) with viscosity of 1 centipoise was used in this analysis. The flow was taken to be steady, with an inlet velocity of 2.1 m/s (6.9 ft/s), approximately equiva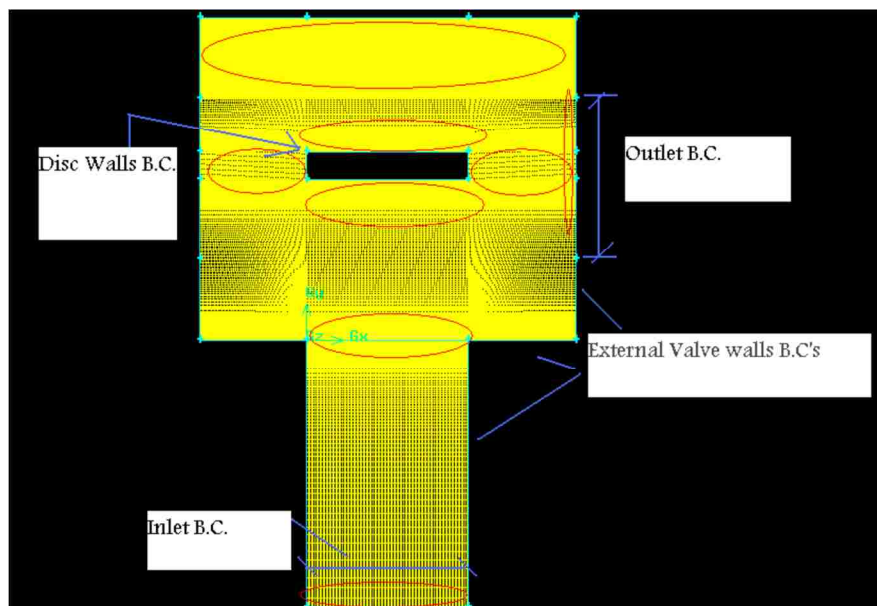lent to 34 $m^3$/hr (150 gpm). This is the typical flow rate seen with a 76.2 mm (3 in.) pump. This also reflects the amount of fluid that would be

by-passed by a typical IRV during a complete by-pass situation. Fig. 4.2 also illustrates the boundary conditions that were implemented. It was further assumed that the ERV disc would be at its maximum lift position of 76.2 mm (3 in.) in a complete by-pass situation. Turbulence intensity was set at 5% (medium turbulence). The hydraulic diameter was set to 76.2 mm (3 in.). The ERV walls were defined with no slip wall boundary conditions.

Several test cases were set up to evaluate the effect of the different settings of interest mentioned above. A summary of the main parameters in the simulations is provided in Table 4.1.

| 2D Simulation Cases | | | Boundary conditions | | Relaxation factors | | | Numerical parameters | | |
|---|---|---|---|---|---|---|---|---|---|---|
| Case | Turb. model | Simulation domain | Inlet | Outlet | u,v | p | $k,\varepsilon,\omega$ | Discr. order | Tol. | # iter. |
| A | $k$-$\varepsilon$ | no extension | vel. | outflow | .6 | .3 | .8 | 1 | $10^{-3}/^{-6}$ | - |
| B | $k$-$\varepsilon$ | short extension | vel. | outflow | .6 | .3 | .8 | 1 | $10^{-3}$ | 93 |
| C | $k$-$\varepsilon$ | short extension | vel. | outflow | .7 | .2 | .7 | 2 | $10^{-4}$ | 283 |
| D | $k$-$\varepsilon$ | short extension | vel. | outflow | .6 | .2 | .7 | 2 | $10^{-4}$ | 545 |
| E | $k$-$\varepsilon/\omega$ | short extension | vel. | outflow | .6 | .3 | .8 | 1 | $10^{-3}$ | 76 |
| F | $k$-$\varepsilon$ | short extension | pres. | pres. | .6 | .3 | .8 | 1 | $10^{-4}$ | 323 |
| G | $k$-$\varepsilon$ | conv-div nozzle | pres. | pres. | .6 | .2 | .7 | 2 | $10^{-4}$ | 862 |
| H | $k$-$\varepsilon$ | conv-div nozzle | vel. | outflow | .6 | .2 | .7 | 2 | $10^{-4}$ | 510 |
| I | $k$-$\varepsilon$ | conv-div nozzle, extended exits | pres. | pres. | .6 | .2 | .7 | 2 | $10^{-4}$ | 345 |
| J | $k$-$\varepsilon/\omega$ | conv-div nozzle, short extension | pres. | pres. | .6 | .2 | .7 | 2 | $10^{-4}$ | 383 |

Table 4.1: Test cases for 2D model of ERV

Case A: Initial simulations were performed using first order upwinding. The inlet boundary conditions were set as a velocity inlet, with velocity of 2.1 m/s (6.9 ft/s). The outlet boundary condition was specified as outflow. The flow variables were initialized from the inlet velocity with a value of 2.1 m/s (6.9 ft/s). For the equation residuals, the

25

convergence tolerance was set at $1.0\times10^{-3}$ for the continuity and x- and y-momentum equations. The convergence tolerance for the turbulent kinetic energy and dissipation was set at $1.0\times10^{-6}$. These tolerances are the default values in ANSYS Fluent. The $k$-$\varepsilon$ turbulence model with near-wall treatment was used since it gives fairly accurate results in the majority of uncomplicated fluid flows, and is the most popular model for industrial simulations. Under-relaxation factors are listed in Table 4.1. With these settings, the residuals stabilized after approximately 100 iterations, but did not fall below the specified tolerance within 500 iterations, as seen in Fig. 4.3.
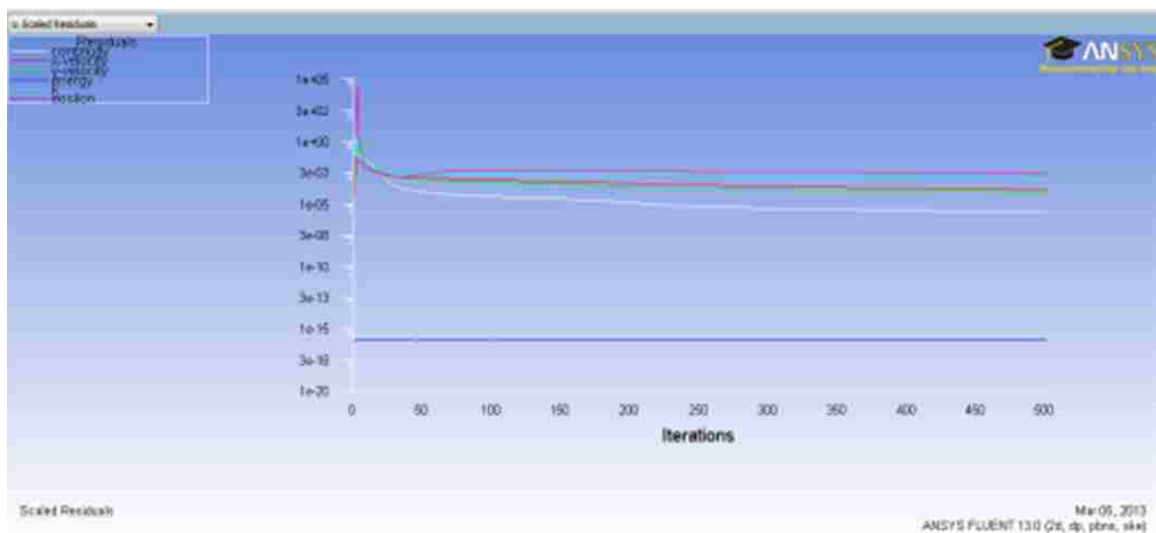


Fig. 4.3: Scaled residuals (Case A)

This simulation was initially carried out on a coarser mesh than shown in Fig. 4.2 and, although the solution did not converge, it suggested certain modifications to the mesh. The mesh in Fig. 4.2 is the result of these modifications. The numerical set up was evaluated by examining: the contours of velocity magnitude; contours of the x- and y-components of velocity; velocity vectors and pressure contours. The velocity magnitude contours are illustrated in Fig. 4.4, showing the regions of separation that occur because of the sharp corners at the junction between the inlet channel and the main body of the

valve. The acceleration of the fluid as it is deflected by the disc is also captured. However, this plot clearly suggests that the exiting flow is not aligned with the x-axis, which is the fundamental assumption of the outflow boundary condition.
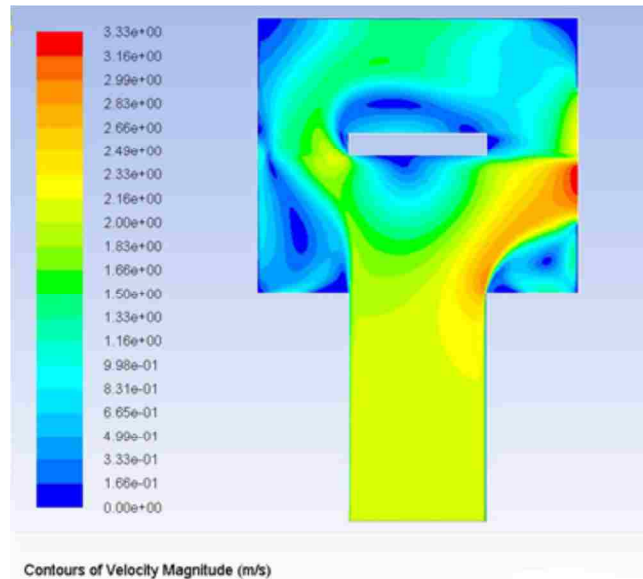


Fig. 4.4: Contours of velocity magnitude (Case A)

The static and dynamic pressure distributions, shown in Fig. 4.5 and Fig. 4.6 respectively, were also assessed. As expected, the static pressure is highest on the frontal face of the disc. The contours in Fig. 4.6 show that the highest dynamic pressure occurs where the velocity is at its highest as it goes around the sharp corner before it exits the valve.

Contours of Static Pressure (pascal)
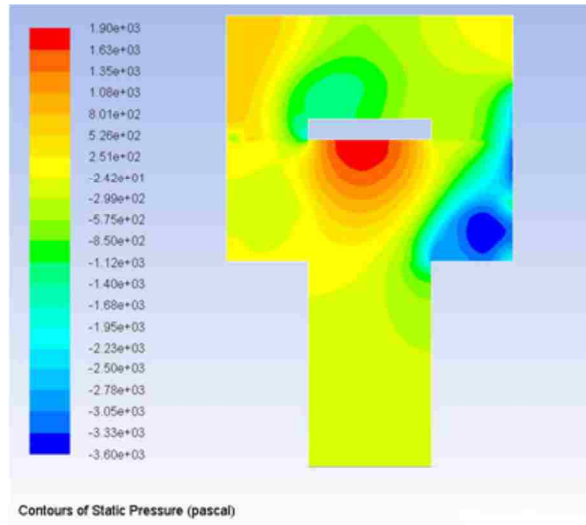
Fig. 4.5: Contours of static pressure (Case A)



Contours of Dynamic Pressure (pascal)

Fig. 4.6: Contours of dynamic pressure (Case A)

Case B: The analysis of case A indicates that there is a need to incorporate an outlet port on the discharge side of the valve to allow implementation of the outflow boundary condition at the exit of the domain. This also represents a more accurate simulation of the return to tank portion of the valve through a small extended pipe. The ERV was re-

designed and the multi-block method was used to generate the mesh. A structured quadrilateral mesh was still utilized in this analysis. The re-designed ERV model is shown in Fig. 4.7. Th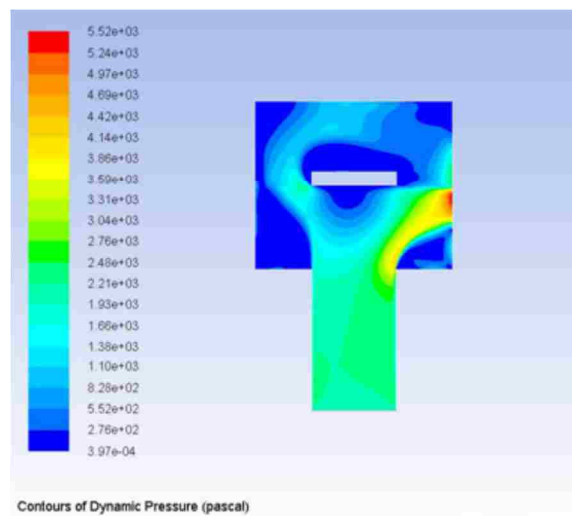e arrows schematically indicate flow direction and the elliptical curves identify regions where particular attention is required due to large gradients in the flow variables.
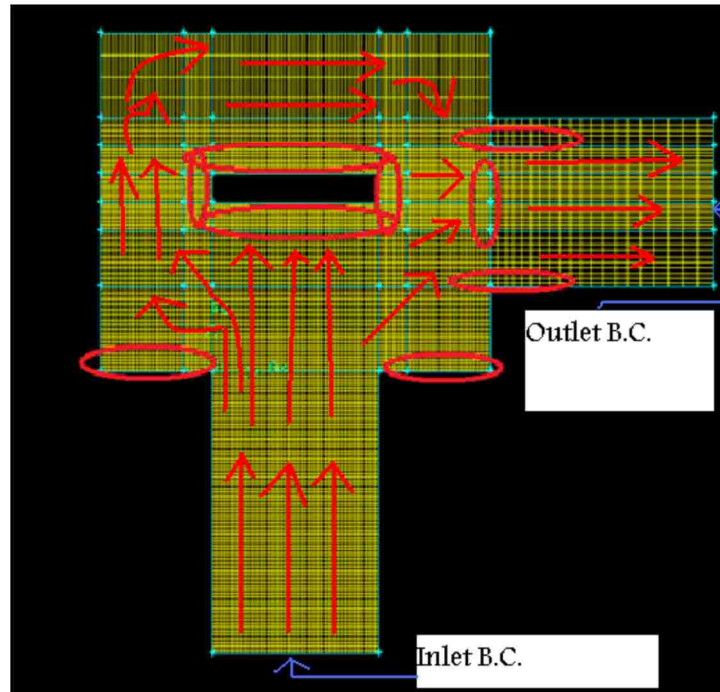


Fig. 4.7: Re-designed ERV model with multi-block mesh (Case B)

If an outflow boundary condition is applied at the outlet, it is imperative that there is no back flow on the outlet plane. Therefore different outlet lengths, from 101.6 mm (4 in.) to 355.6 mm (14 in.), were investigated to determine the proper outlet length to ensure a correct outflow condition was being investigated and to mitigate potential back flow. Schematics of the different nozzle lengths are illustrated in Fig. 4.8. For these simulations, all boundary conditions (with outflow at the extended outlet plane) and

parameter settings in case A were retained, except that the tolerance for the turbulent kinetic energy and dissipation residuals was set at $1.0 \times 10^{-3}$. For the domain with the short discharge extension (101.6 mm), the solution converged in 93 iterations, as shown in Fig. 4.9. Other extended discharge lines also produced converged solutions.
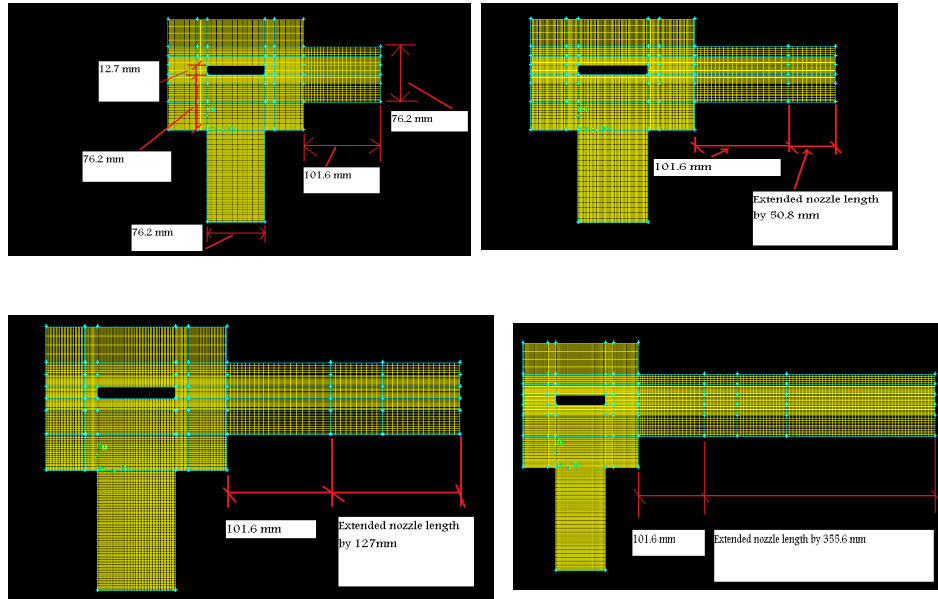


Fig. 4.8: Discharge nozzle extensions
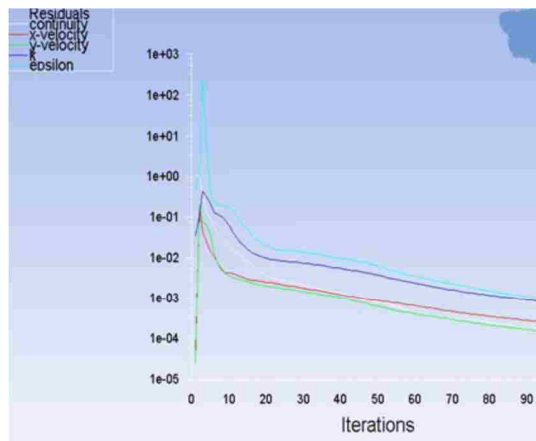


Fig. 4.9: Scaled residuals (Case B)

30

The velocity magnitude contours for the short extended nozzle are shown in Fig. 4.10. As the fluid enters the valve, some of the fluid particles accelerate to pass over the sharp corner and move towards the discharge channel. Other fluid decelerates as it enters the larger valve region and encounters the disc. This flow behaviour is expected due to the physical characteristics in the valve and the natural ability of the flow to take the path of least resistance.



Contours of Velocity Magnitude (m/s)
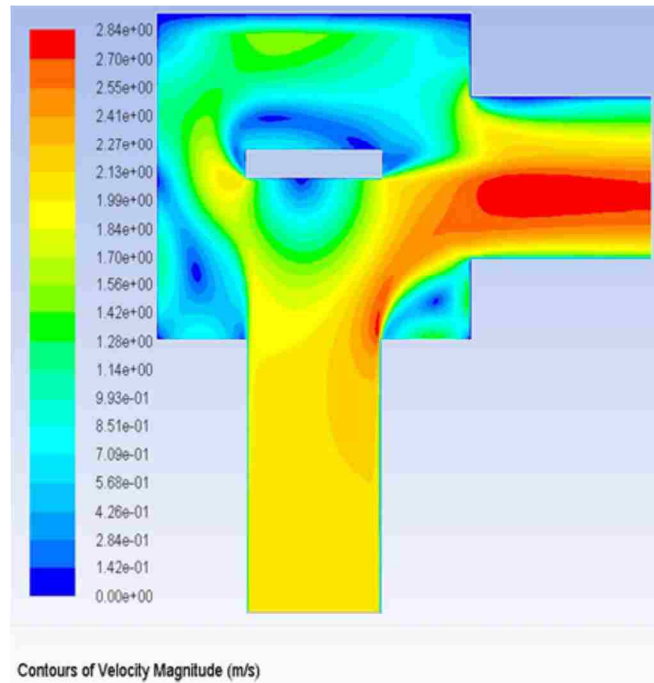
Fig. 4.10: Contours of velocity magnitude (Case B - 101.6 mm extension)

Velocity vector plots and contours of turbulence (kinetic energy and dissipation), turbulent intensity and static/dynamic pressure show that the change in valve geometry and mesh features using a multi-block method facilitate reduced computational time and improve accuracy in the CFD simulation. Although longer extensions to the discharge channel showed boundary-layer development along the channel walls and slightly longer recirculating zones at the entrance to the discharge, the effect on the valve disc was

negligible. Thus, the valve with the 101.6 mm discharge extension was retained for subsequent simulations.

Case C: Several parameters were changed to obtain more accurate results. The discretization of the convective terms was changed from first order upwind to second order upwind for momentum, turbulent kinetic energy and turbulent dissipation rate equations. The relaxation factors for pressure, momentum and turbulent kinetic energy were changed as listed in Table 4.1. The convergence tolerances were also adjusted from $1.0 \times 10^{-3}$ to $1.0 \times 10^{-4}$ for continuity, x-velocity, y-velocity and turbulent parameters. The higher order upwinding and tighter tolerance produced more accurate results, with the solution converging after 283 iterations.

Case D: To assess only the effect of under-relaxation factors, the momentum equations relaxation factor was reduced from 0.7 to 0.6 while others were kept the same as in case C. Under these conditions, the solution converged at 545 iterations. The solutions from cases B and D are compared in Fig. 4.11 using contours of velocity magnitude.
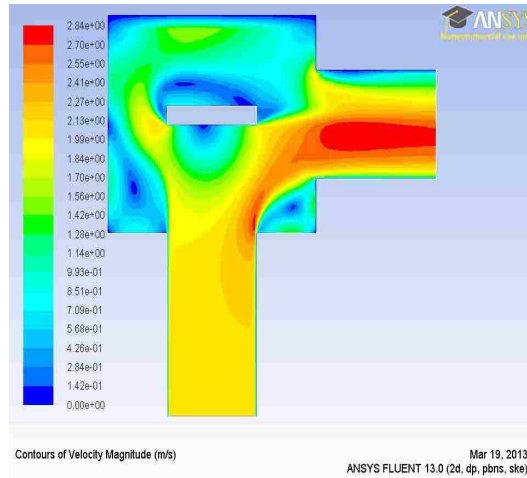
(Case B)
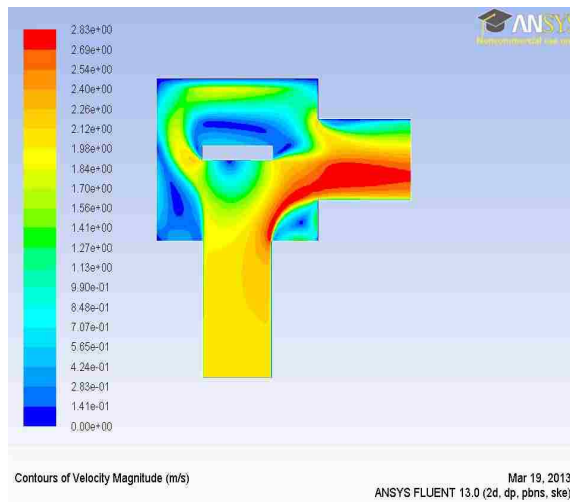


(Case D)

Fig. 4.11: Comparison of velocity magnitude contours (Cases B and D)

It can be observed that there is very little distinction in these contours in the region around the disc, although the discharge is modified. Pressure contours (dynamic and static) and velocity vectors were also compared for cases B and D (93 iteration converged solution vs. 545 iteration converged solution). There were no significant

differences in these plots. Therefore it was concluded that these changes in the parameters did not make a significant difference.

Based on these preliminary investigations, it was decided to move forward with the following parameters, taking into account the desired accuracy and the computational time required for each simulation:

- convergence tolerances: $1.0 \times 10^{-4}$;

- relaxation factors: pressure = 0.2; default values for momentum, turbulent kinetic energy, turbulent dissipation and turbulent viscosity;

- spatial discretization: second order upwinding for momentum, turbulent kinetic energy, turbulent dissipation; standard for gradient and pressure;

- turbulence model: $k$-$\varepsilon$ with near-wall treatment.

These parameters correspond to case C and yielded a solution after 283 iterations. The first order solution with tolerance $1.0 \times 10^{-3}$ and convergence at 93 iterations and the second order solution with tolerance $1.0 \times 10^{-4}$ and convergence at 283 iterations are compared in Fig. 4.12. There appears to be no significant difference in the contours for these two simulations. Velocity vectors and velocity magnitude contours were also investigated, leading to the same conclusion as above.
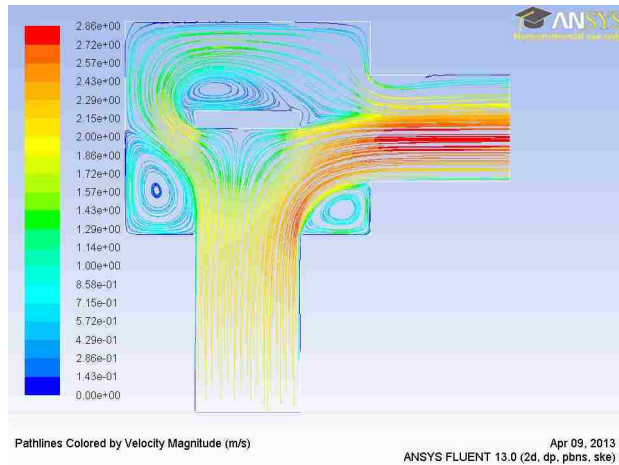
(Case B)
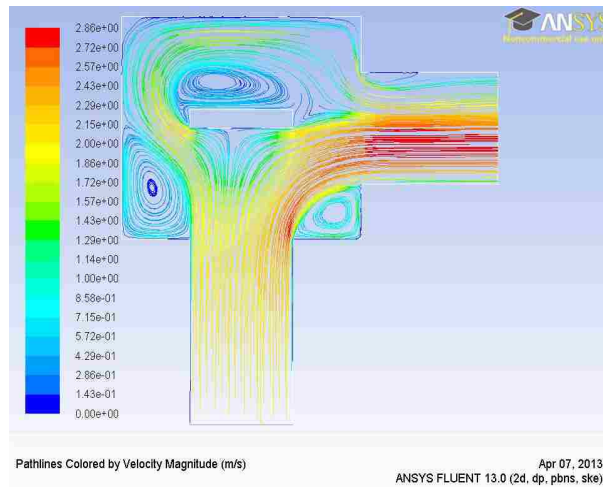


(Case C)

Fig. 4.12: Streamlines coloured by velocity magnitude (Cases B and C)

The wall Y+ value is usually used to determine whether the mesh is fine enough to capture the wall effects. Generally speaking, when using the $k$-$\varepsilon$ turbulent model, a Y+ range of approximately 30 to 50 is desired to effectively capture the boundary layer. Figure 4.13 illustrates the Y+ on the disc for case C, showing Y+ is close to 30 at the

bottom of the disc and increases from 30 to slightly above 50 on the side disc faces. The Y+ value at the top of the disc does not appear to be correct. The Y+ on the valve boundary walls was also investigated and is illustrated in Fig. 4.14. Along the inlet section, the Y+ value ranges from slightly above zero at the entrance to almost 100 before the fluid enters into the ERV body. The Y+ values on the ERV outer faces were also high, in the vicinity of 100 to 600. The separation, recirculation and reattachment occurring in the valve at these locations may be the cause of the high values of Y+. The separation and recirculation make it more difficult to capture the boundary layer of the flow, where the velocity of the fluid increases from zero to some finite value across a very short distance normal to the wall to form the boundary layer.
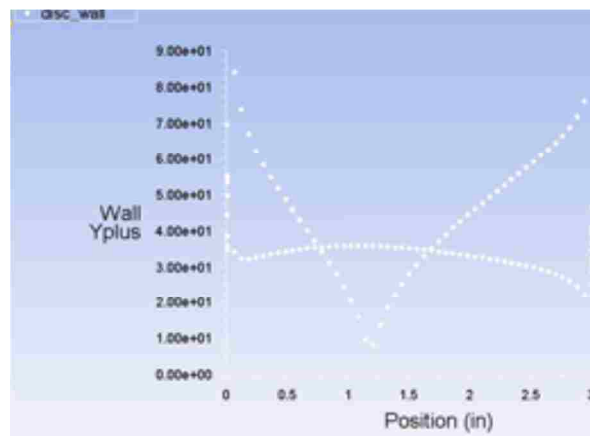


Fig.4.13: Y+ on disc walls
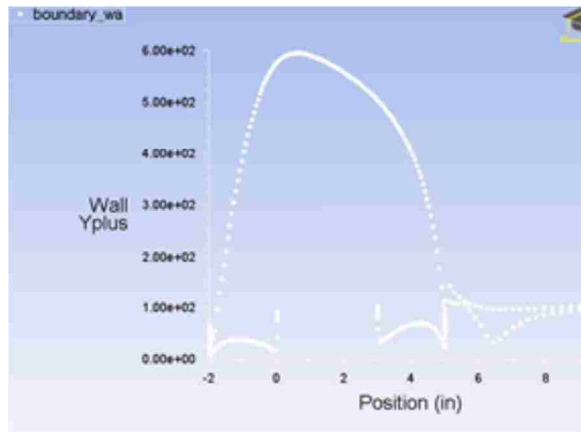
Fig. 4.14: Y+ on ERV boundary walls

Case E: The streamlines predicted by the $k$-$\varepsilon$ and the standard $k$-$\omega$ turbulence models are compared in Fig. 4.15. Both solutions incorporated the default Fluent parameters used in case B. There appears to be no significant difference between the two models when observing these contours.

*(k-ε)*



*(k-ω)*
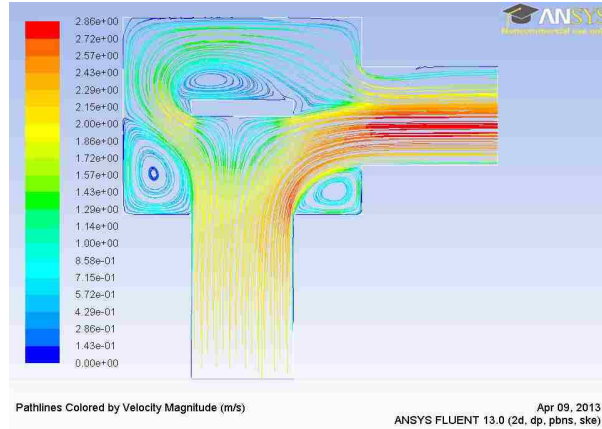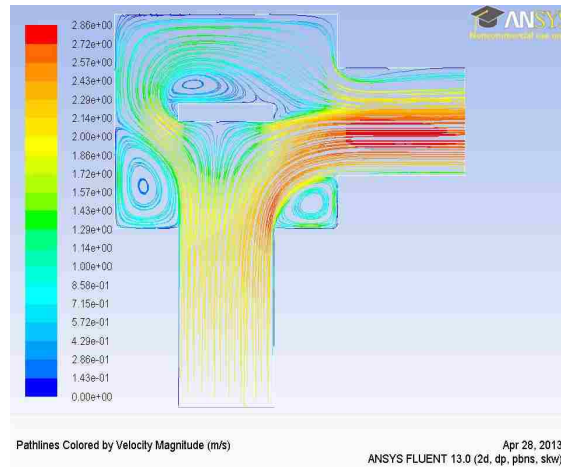
Fig. 4.15:  Streamlines coloured by velocity magnitude – *k*-ε vs. *k*-ω turbulence models

Since the turbulence model has been changed, it is prudent to check the flow in the discharge section to ensure no back flow is present. To do this, five vertical cross-sections were created in the outlet region of the ERV, as shown in Fig. 4.16. The velocity vectors on these vertical cross-sections were plotted and the findings show that near the entrance of the outlet channel, around x = 6, 7 and 8, there is recirculation (negative

38

velocities) due to flow separation. However, at x = 9 the velocities are all positive giving

a strong indication that no back flow is present near the exit of the outlet of the valve.
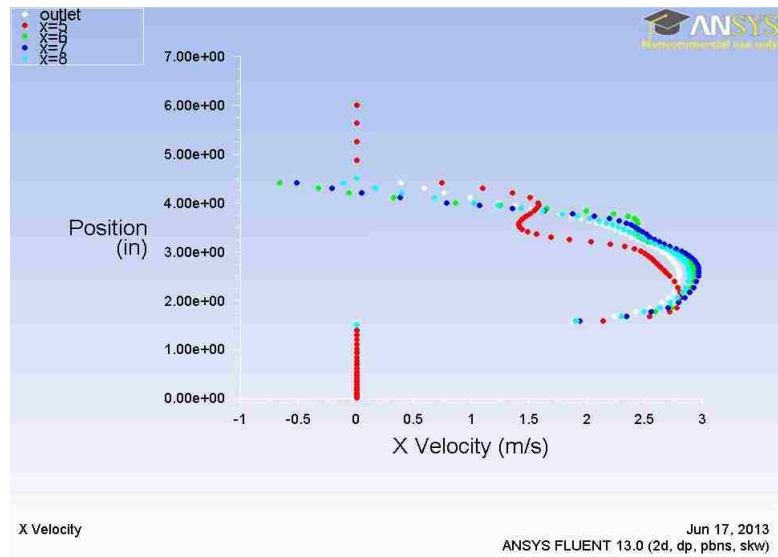


(a)
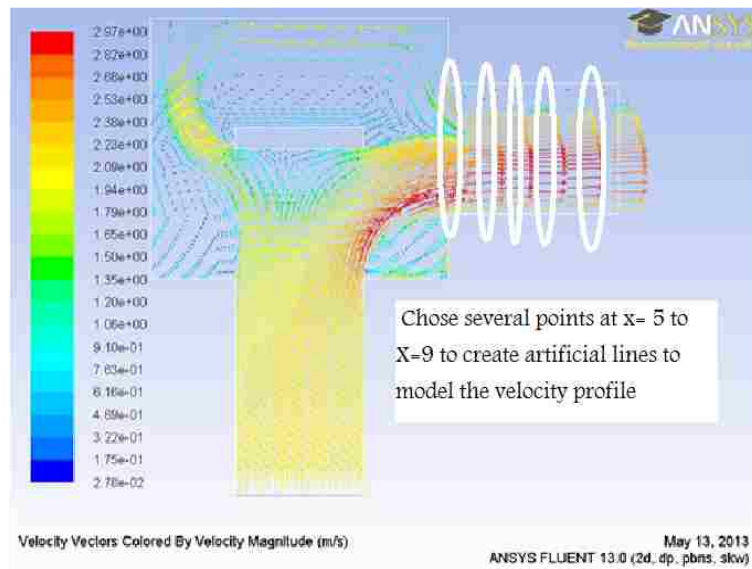


(b)

Fig. 4.16: Check for back flow in the discharge line

Case F: The velocity inlet and outflow outlet boundary conditions have been used in all the above simulations. However, it is important to check whether the velocity inlet condition can be reproduced while imposing pressure inlet and pressure outlet conditions, since these are the type of boundary conditions that can be extracted for a typical industrial installation. A pressure inlet value of 2 kPa (0.3 psi) was estimated from the velocity inlet profile and the dynamic pressure contours at the inlet. A pressure outlet condition was imposed at the outlet boundary and default values were used for the various flow and numerical parameters except the tolerances which were set at $1.0 \times 10^{-4}$. When comparing the velocity magnitude contours with case C, it was observed that the two sets of contours match fairly well, as demonstrated in Fig. 4.17. However, the predicted velocity at the inlet was approximately 1.50 m/s (4.9 ft/s), which is less than original input value of 2.1 m/s used in Case C. Further investigation was conducted to determine the cause of this discrepancy.
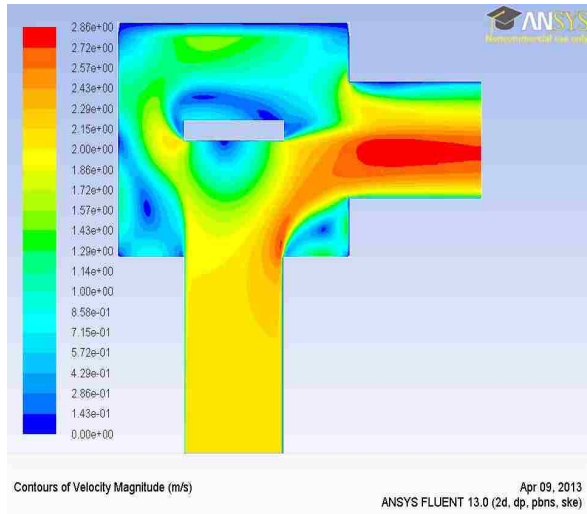
(Case C)
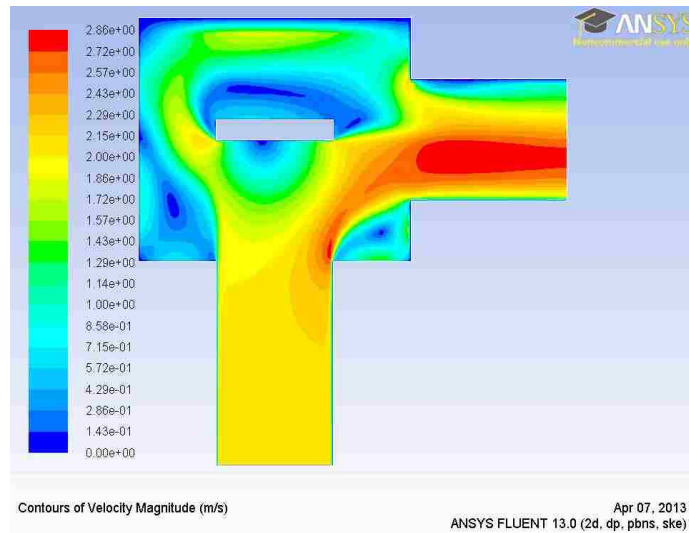


(Case F)

Fig. 4.17: Pressure inlet/outlet BC's vs inlet/outlet BC's (Cases C and F)

Case G: After further extensive investigation, it was apparent that the ERV should be viewed like a converging-diverging nozzle, where the seat and disc creates an orifice. During operation of the valve, the flow area should vary from zero when the valve is

closed to a maximum, less than or equal to the inlet area, when fully opened. The valve geometry used in the above cases displays a divergent-convergent section. This indicates that the orifice area, referred to as the throat or curtain area (area between bottom of the disc and the inlet nozzle seat), is larger than the inlet and outlet port areas. This completely defies the theory of valves. According to Bernoulli's theorem, when a fluid under pressure is accelerated through an orifice such as a valve, the static head is converted to the velocity head resulting in a pressure drop. If the area is smaller at the inlet and outlet, the velocity will decrease as the flow enters the throat area. This could have an adverse effect on how the flow responds as it passes the valve throat, as shown in Fig. 4.18.
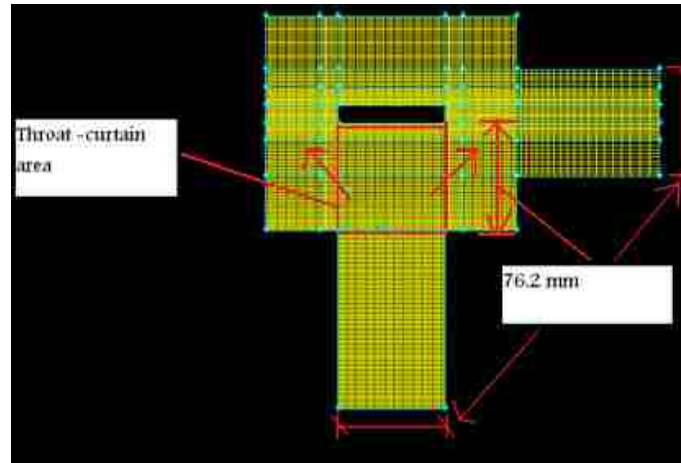
(a)
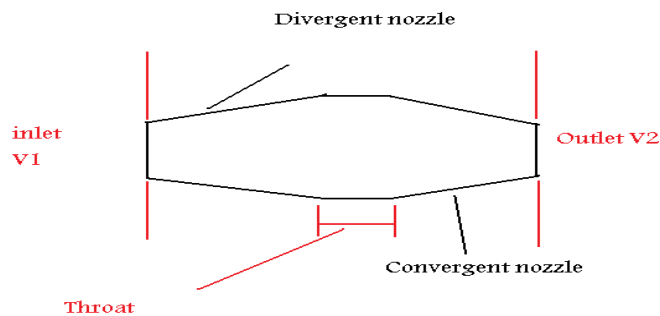


(b)

Fig. 4.18: Schematic of divergent-convergent model, incorrectly depicting an ERV

It would be beneficial if the throat or curtain area (orifice) were much smaller than the inlet and outlet areas. To account for this, the curtain area has to be made smaller. This can be done by extending the valve nozzle seat as illustrated in Fig. 4.19. The distance between the bottom of the disc and the inlet into the ERV (curtain distance) was changed from 76.2 mm (3 in.) to 12.7 mm (0.5 in.), thereby decreasing the throat area from $5806.4\pi$ mm$^2$ to $967.7\pi$ mm$^2$. See Appendix B for calculations.
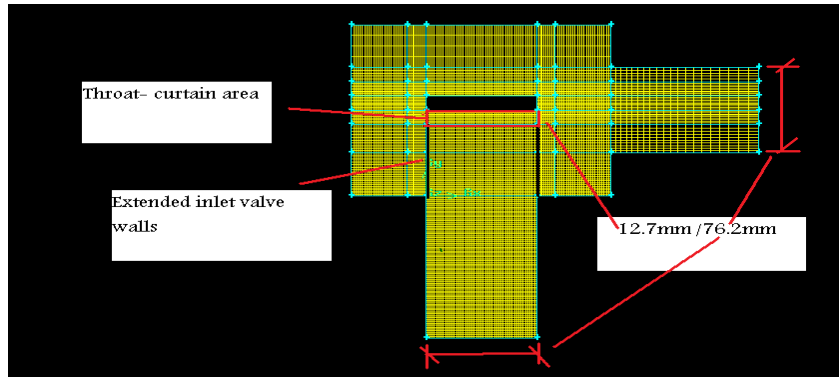
(a)
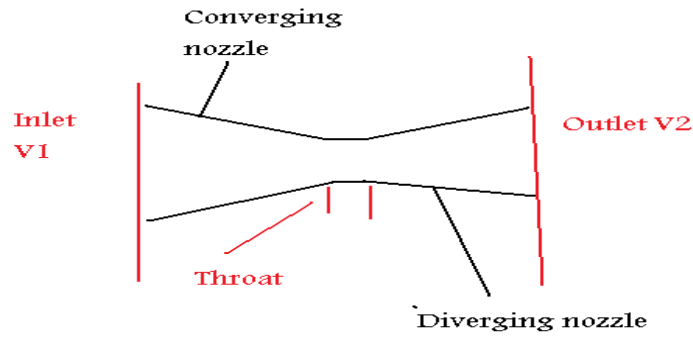


(b)

Fig. 4.19: Schematic of convergent-divergent nozzle, correctly depicting a valve

analogous to an ERV

Following the same setup and procedure as in case F with the short extended outlet nozzle and using this new valve configuration which models the ERV as a convergent-divergent nozzle, the pressure inlet/outlet conditions reproduce the correct velocity inlet.

Case H: The converging-diverging model that was used in case F was further investigated using velocity inlet and outflow boundary conditions, and the results are compared with case F in Fig. 4.20.
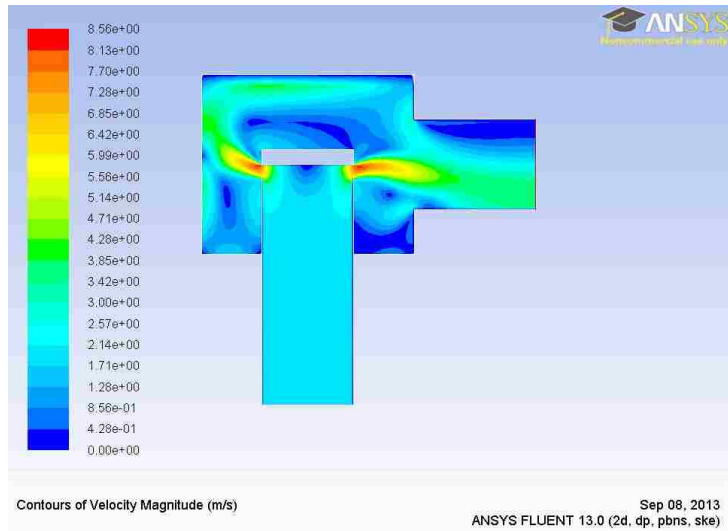


(Case G)
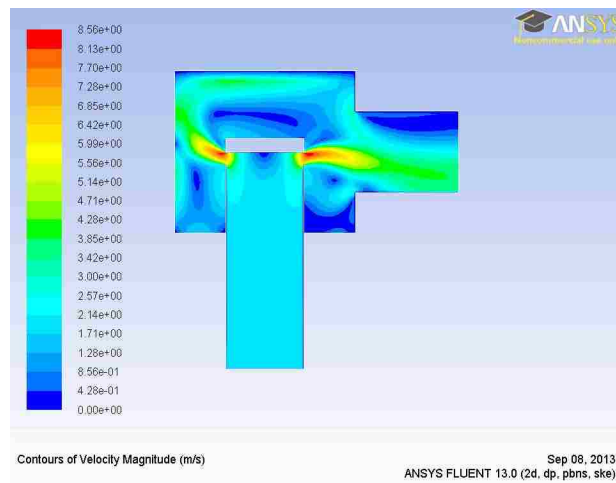


(Case H)

Fig. 4.20: Velocity magnitude contours (Cases G and H)

Case I: With the new geometry it is necessary to check for possible back flow in the outlet nozzle and to see where the flow reattaches after it separates at the sharp corners in the ERV. To verify that there is no backflow on the outlet plane, the discharge nozzle length was extended by 50.8 mm (2 in.), 127 mm (5in.) and 355.6 mm (14 in.), as shown in Fig. 4.8 and displayed below for convenience. However, the new configuration being tested includes the curtain described above, which are not shown in Fig. 4.8.
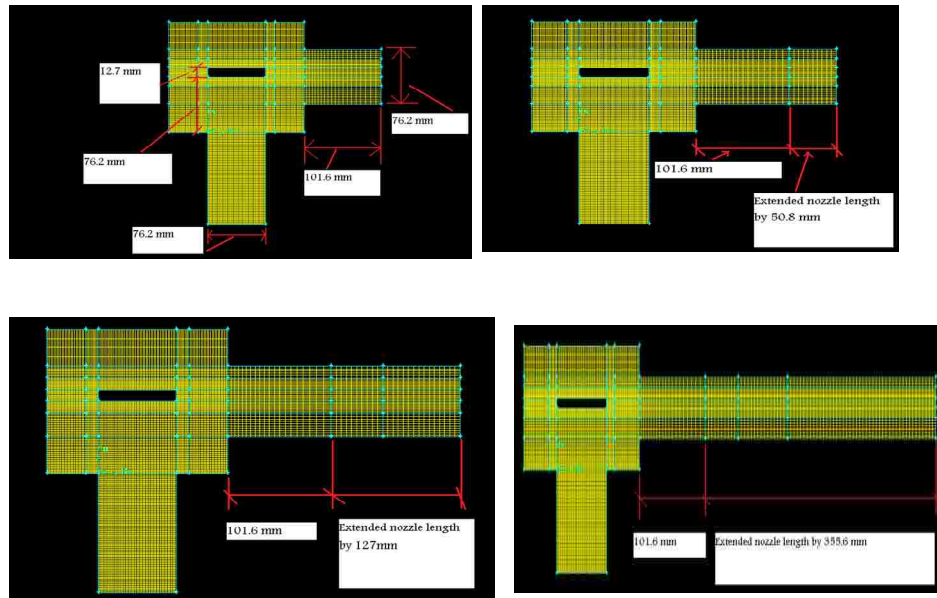


Fig. 4.8: Discharge nozzle extensions

Pathlines, velocity magnitude contours and velocity vectors were plotted to determine where the recirculation occurs and where the flow reattaches. A vertical line was drawn at all new nozzle lengths in order to capture velocity and dynamic pressure profiles beyond the 101.6 mm (4 in.) nozzle length in the extended valves. Profiles like

those shown Fig. 4.22 indicate that the recirculation and reattachment points are captured more effectively by extending the nozzle. However, this investigation was solely done to ensure that no back flow was occurring and to determine if the outlet length of the valve needed to be longer to capture this feature. It was observed that by extending the discharge length, no back flow was present. This confirmed that the original outlet length was adequate for further 2D and 3D analysis.



- Determined their was separation, thus back flow is occurring in nozzle

- Extended nozzle an additional 14 inches which changed length to 18inches total

- Re-attachment occurred at approximately 9 to 10 inches in nozzle length
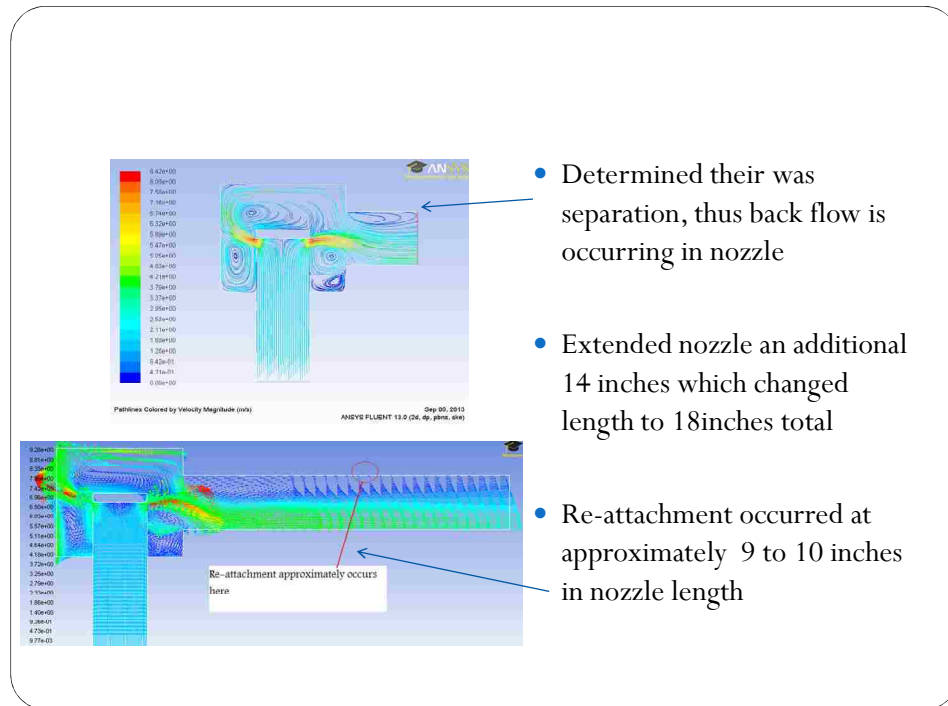
Fig. 4.21: Outlet condition check – velocity vectors

- Does not capture recirculation
- Does capture slight recirculation bubble
- Dynamic pressure larger especially at 1.5 to 2"
  section of nozzle (Extended nozzle)-7000 Pa
  compared to 10000 Pa
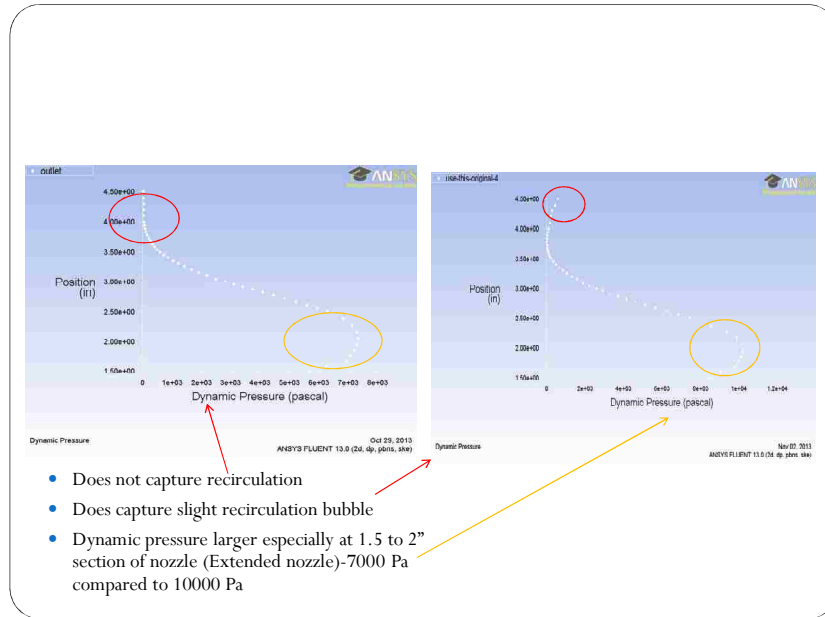
Fig. 4.22: Outlet condition check – dynamic pressure profiles

Case J: The $k$-$\varepsilon$ (standard and realizable) and $k$-$\omega$ (standard) turbulent models were investigated and compared using the new geometry described above. The results between the models were not significantly different. However, for the 3D simulations, a model will be required that can handle adverse pressure gradients and give reasonably accurate results with boundary layer flow. The $k$-$\omega$ turbulent model was selected for subsequent simulations since the 3D ERV and the 3D IRV geometry (bends/corners/etc.) will be more complicated.

## 4.3.     Three-Dimensional Simulation of the ERV

A three dimensional model of the ERV was developed using the same parameters in Fluent with the $k$-$\omega$ turbulent model as in case J above. Figure 4.23 shows the hybrid mesh that was used for the simulation, comprised of structured hexahedral and unstructured tetrahedral elements with approximately 77,564 nodes and 186,831 mixed

cells. Dynamic pressure contours are shown in Fig. 4.24. This shows the surfaces on which the contours of dynamic pressure are plotted. Fig. 4.24 also displays a central plane cross-section of the valve and shows that the high velocity fluid that is squeezed between the valve disc and the curtain contributes to the region of high dynamic pressure.
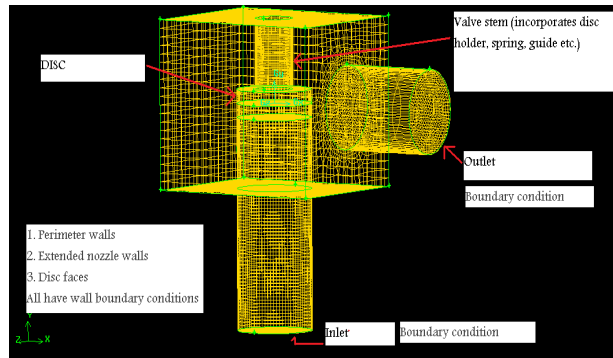


Fig. 4.23: Mesh for model of 3D ERV
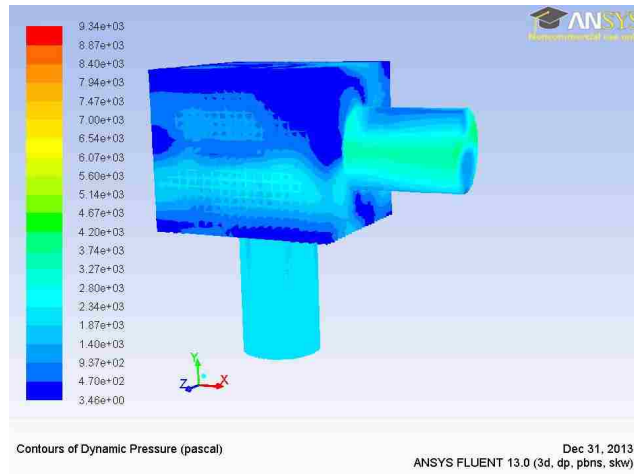
a)
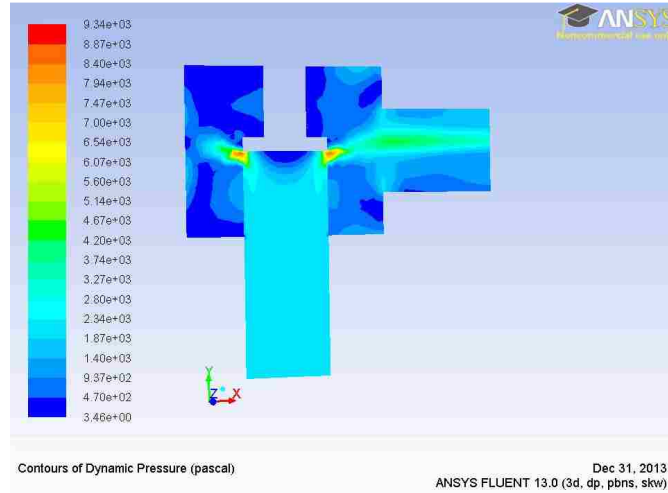


b)

Fig. 4.24: Dynamic pressure contours of 3D valve model

# CHAPTER 5.   INTERNAL RELIEF VALVE

## 5.1.      Introduction

The internal relief valve (IRV) is a safety device which is essential in providing over-pressure protection to the internal gear pump. The IRV device not only protects the pump from catastrophic failure but also serves as a protection measure for workers and the general public in the event of such a failure. In this chapter, a computational model for the fluid flow through an IRV is developed and used to investigate the features of the flow through the valve at fully open condition. In particular, the CFD model provides detailed information on the velocity and pressure fields within the valve. Analysis of the results leads to a fuller understanding of the valve operation and suggests potential modifications for improvement of the IRV.

## 5.2.      Determining IRV pressure setting

The relationship between the internal gear pump and the IRV is based on the differential pressure that the pump experiences and the capacity/flow that the pump produces. The IRV has a predetermined setting at which the valve will be fully open, thus creating a full by–pass situation in the pump. In this scenario, the fluid will circulate within the pump and not leave through the discharge. The IRV setting is determined from an optimum point selected on a graph of the differential pressure vs. pump capacity, and by a line intersecting the horizontal x-axis. For example, as shown in Fig. 5.1, the optimum point is generated by intersecting the pump capacity 14 m$^3$/hr (60 gpm) and the pump differential pressure 552 kPa (80 psi). Once the optimum point is obtained, a diagonal line is drawn through the optimum point and parallel to the differential pressure

line on the graph. The full by-pass pressure is set at the point where this diagonal line intersects the horizontal axis. In practice, most pump internal relief valves are set at approximately 172 kPa to 207 kPa (25 to 30 psi) above the differential pressure setting. However, the size of the pump, which influences capacity/flow capabilities, is often used as a measure to change this range to a higher value. It is important to note that the differential pressure at which the pump is sized at is representative of the cracking pressure. Therefore in the example discussed above, 552 kPa (80 psi) which is the differential pressure is the same value as the cracking pressure.
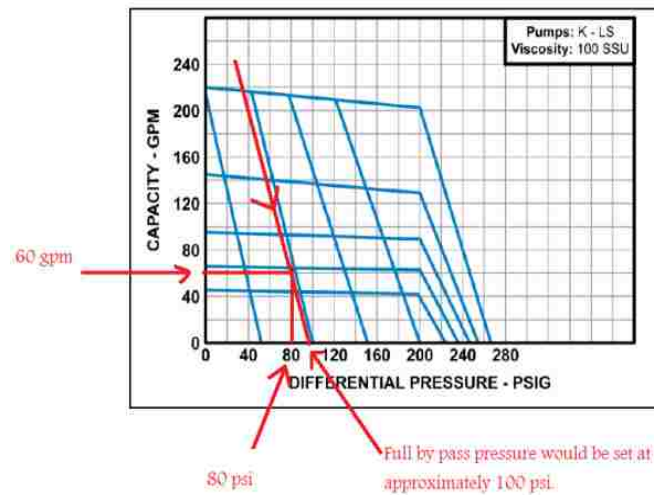


Fig. 5.1: Viking safety relief valve performance curve (K-LS size pump) [11]

(by permission of Viking Pump Inc.)

52

## 5.3.        Research Motivation

Advancement in product development is of utmost importance in the practical engineering world. Research plays a critical role in this type of engineering environment. In the present context, for companies like Viking Pumps Inc., exploring potential techniques for improved IRV performance is key in moving forward with better products. The goal would be to reduce the range from cracking to full by-pass pressure of the IRV as illustrated in Fig. 5.2. By achieving this goal, numerous direct benefits may be realized, as is further discussed.

To date very little is known about the poppet movement inside the internal production relief valve. A couple of studies have been performed on prototypes for new designs, but these have not made it to production thus far. There have been no studies done on production IRV's to validate poppet movement.  Once the IRV is subjected to an over-pressure situation, movement of the poppet cannot be confirmed precisely in a practical sense since the poppet is completely enclosed in the IRV. An experimental study would require a transparent model and rather sophisticated measuring devices, thereby incurring considerable cost. A CFD analysis will provide detailed flow data from which it is possible to get a better understanding of the poppet movement and help to relate the flow and differential pressure to a specific poppet lift position.
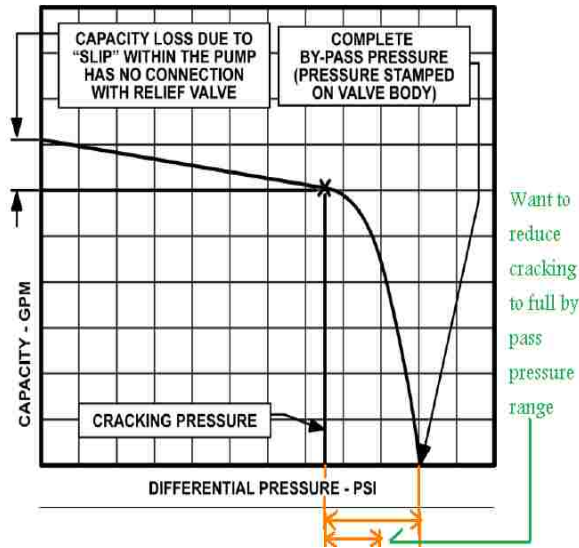
Fig. 5.2: Relationship between cracking and full by-pass pressure [11]

(by permission of VikingPump Inc.)

By reducing the pressure range from cracking to full by-pass pressure, the fluid would by-pass earlier. This would lead to significant improvements in valve operation. It is anticipated that a reduction in the cracking to full by-pass range could be achieved by modifying the IRV design, changing the functionality of a component, changing materials or through some other mechanism that improves the flow characteristics which affect the forces acting on the poppet.

## 5.4.    Benefits from Improved Relief Valve Performance

There are many benefits to be gained from improved IRV performance by reducing the pressure range (cracking to full by-pass):

1.  Reduced horsepower requirement:

    Pumps are sized based on the relief valve setting. By shortening the pressure range from cracking to full by-pass, the IRV setting could be reduced. This would

result in a smaller motor horsepower (HP) requirement to completely open the valve in over-pressure situations. This would generate a huge cost savings especially when larger HP motors are used.

2. Reduction in slippage:

Slippage occurs when thin liquids fall behind the rotor and idler teeth while the pump is running. When this occurs flow will be diminished since you will have fluid slipping past components instead of exiting the pump as the fluid is carried from the suction to discharge port. Slippage gets worst with increased temperature and pressure. With a reduced pressure range, the pump would be subjected to lower pressure. This would be especially helpful in applications with thin liquids and higher pressures where slippage is inevitable. By reducing slippage, the mechanical efficiency of the pump would improve since the fluid would not be lost due to slippage. Also, considering the frequency at which the IRV comes on, with smaller pressure range the spring would be subjected to less pressure/force, and thus have a potential extended life.

3. Avoid damage to pump

If the IRV works properly and efficiently it will help to avoid damage to the pump.

## 5.5.    Internal Relief Specifications

The internal relief valve modeled in this study is a Viking IRV 3-795 series, as shown in Fig. 5.3.   Figure 5.4 illustrates the three-dimensional mathematical data that represents the actual IRV in Fig. 5.3.



Fig. 5.3: Cross-section of the 3-795 series Viking IRV

(by permission of Viking Pump Inc.)
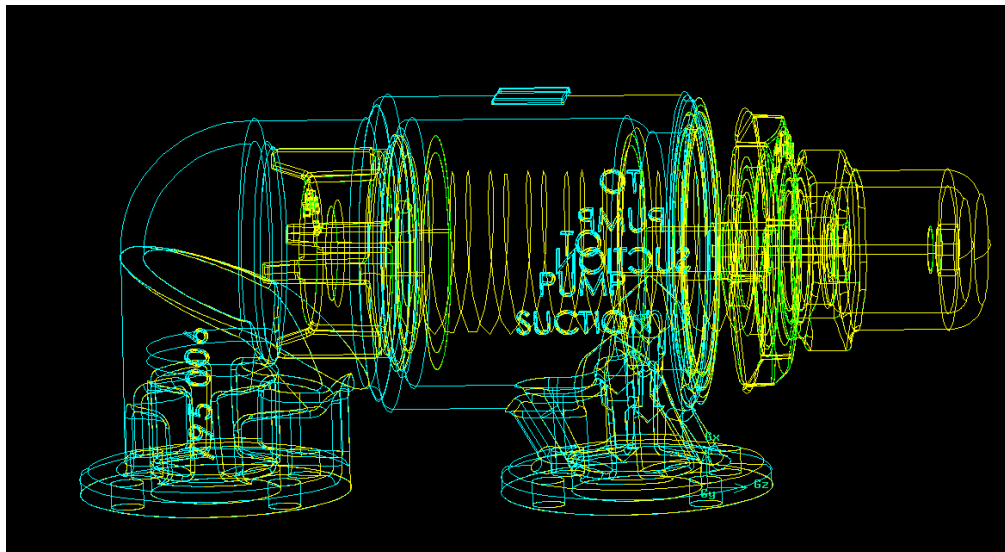


Fig. 5.4: 3D mathematical representation of 3-795 series IRV

The internal relief valve is composed of several components which make up the complete assembly. Figure 5.5 illustrates these components.
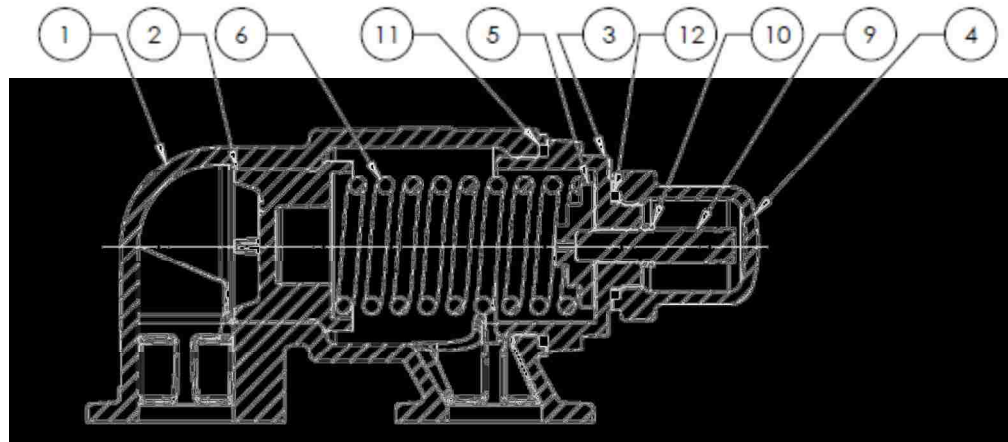
Fig. 5.5: Cross-section of 3-795 series IRV

**Item 1** is the relief valve body which encases all of the other internal components (Items 2 through 12). **Item 2** is the poppet, which is one of the most important components on the relief valve. The poppet helps to relieve pressure by sliding open in over-pressure situations, allowing the fluid to pass through the IRV and re-circulate in the pump. Once the over-pressure situation drops below the spring setting, the poppet closes and blocks flow through the IRV. **Item 3** is the bonnet (RV cap) which encloses the back of the spring and spring guide. Its main purpose is to hold all the components inside the internal relief valve body. **Item 4** is the adjusting screw cap which covers and protects the adjusting screw apparatus. **Item 5** is the spring guide which helps the spring to react in the horizontal direction as the spring is subjected to compression and then returns to its elastic initial state. **Item 6** is the spring, which is the most important component in the IRV assembly. The spring setting will dictate when the poppet moves in an over-pressure situation by compressing when pressure in the pump rises above the spring setting. **Item 9** is the adjusting screw, which allows adjustments to the spring to whatever desired setting pressure is needed, considering the pressure is in the spring pressure range. **Item 10** is the hex nut (lock nut) which is used to lock the adjusting screw in place once the

pressure setting has been determined. **Items 11 and 12** are gaskets which have the sole

purpose to create a positive seal between two relatively stationary parts. This will prevent

leakage onto the adjusting screw threads and the hex nut.

Since it is assumed that heat transfer is negligible, the valve wall thickness is

irrelevant and the flow region is bounded by the interior wetted surfaces of the IRV.

Components such as the adjusting screw, adjusting screw cap and bonnet were removed

from the model as these will not come in direct contact with the fluid. Figure 5.6 shows

cross-sectional views of the complete IRV and in its design configuration used for the

CFD analysis.
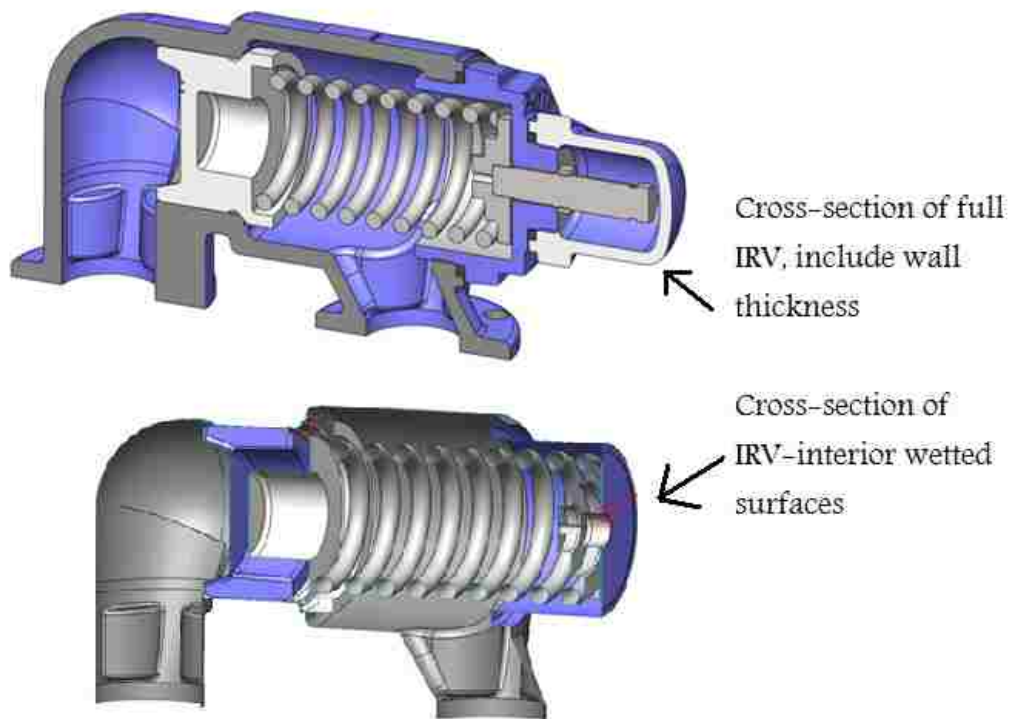


Fig. 5.6: Cross-sections of complete IRV and modeled IRV with interior wetted surfaces

The poppet was offset a distance of 0.63 to 0.64 inches. This offset distance is an

estimate of where the poppet would be at the fully open position, calculated through an

approximate theoretical formula. As there is quite a bit of pressure fluctuation in an over-pressure situation, it is very complicated to predict exactly what position the poppet would be at in the fully open position. Figure 5.7 shows valve with the offset distance used in this thesis.
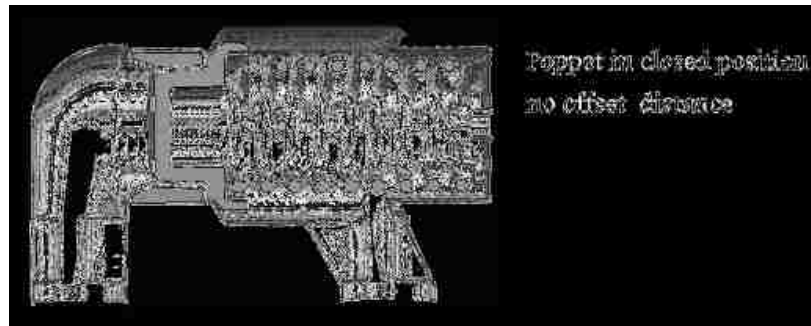


(a)
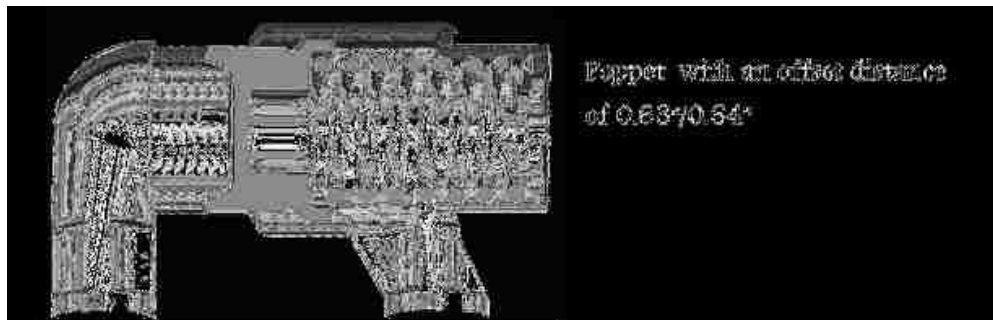


(b)
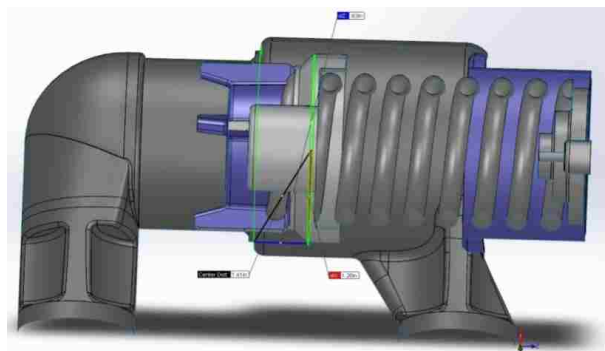


(c)

Fig. 5.7: Poppet in closed position and with offset; 3D offset distance in CFD model

This IRV is typically used on the K and KK size Viking pumps. The selected spring range was 558 kPa to1034 kPa (81 to 150 psi), which is a typical representation of a practical IRV setting in industry. Nominal flow rates of the K and KK size pumps are approximately 17 to 22 $m^3$/hr (75 to 100 gpm). In a full by-pass situation this will be the approximate flow re-circulating within the pump until the over-pressure drops below the spring pressure setting.

## 5.6.    IRV Simulations (Setup)

IRV simulations were performed using the CFD software package STAR-CCM+. The 3D geometry data was imported into STAR-CCM+ using a Nastran file type. Once the file was imported the complete solution domain was partitioned into regions. Edges were split using split angle (60 to 70 degrees) to define boundaries for inlet, outlet, poppet, etc. Geometry cleanup was performed on the model prior to meshing.

The model was meshed using the surface remesher, prism layer mesher and polyhedral mesher available in STAR-CCM+. The surface remesher was applied to the surface mesh and tetrahedral faces were implemented. A prism layer mesh was used to help capture the boundary layer at the walls. The prism layer mesh configuration consisted of the following:

- prism layer stretching = 1.3

- prism layer thickness = 1.5mm

- number of prism layers = 10.

 For meshing the volume, polyhedral cells were implemented in an unstructured configuration. The volume mesh consisted of 1,146,533 cells.

To generate a good volume mesh, a surface mesh with an absolute minimum size of 1.0 mm and an absolute maximum size of 1.5 mm was used. A surface curvature of 36 points was also utilized to aid in define the meshing around the circular features in the IRV. Other mesh parameters include the base size which was set to 0.035052 m. This represents the approximate diameter of the inlet and outlet port of the IRV. The surface growth rate was left at its default value of 1.3. The final mesh can be viewed in Fig. 5.8.
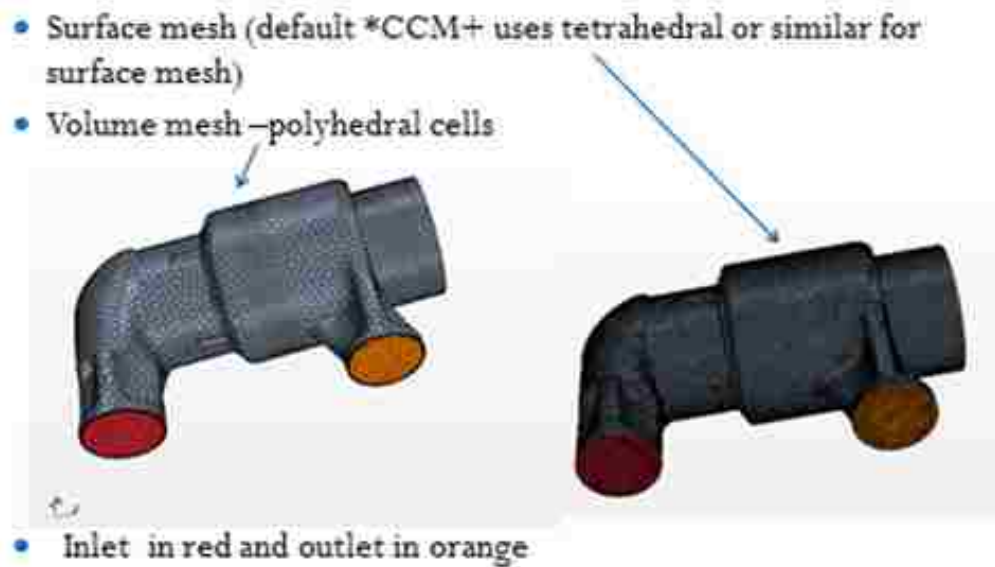


Fig. 5.8: Surface and volume mesh

Both the standard $k$-$\varepsilon$ and $k$-$\omega$ turbulence models were used in the analysis with the "all Y+ wall treatment" option. Ultimately, due to its ability to handle separated flows more effectively, the $k$-$\omega$ turbulence model was used in further analysis. The segregated solver was used. This type of solver allows for superior manipulation of the relaxation factors. The relaxation factors used in the model were as follow:

- for pressure: 0.2

- for velocity: 0.8

-for $k$-$\varepsilon$ or $k$-$\omega$ turbulent viscosity: 0.7

- for $k$ and for $\varepsilon$ or $\omega$ turbulence: 0.5

Both first and second order upwinding of the convective terms were used in the analysis. Unlike many other commercial CFD codes, STAR-CCM+ does not provide the option of using equation residuals to determine whether the iterative solution procedure has converged. Residuals are calculated and can be monitored as the iterations proceed. The  following residuals are calculated: continuity, x, y, z, momemtum, kinetic turbulent energy and dissipation rate. Once the desired residual levels are reached, the simulation can be terminated. The maximum number of iterations has been set at 6000, which acts as a stopping criteria if the residuals have not decreased sufficiently.

The IRV boundary conditions were set as follows. The inlet boundary was set as a pressure inlet and, on the basis of having a spring range of 558 kPa -1,034 kPa (81-150 psi), the inlet (stagnation) pressure was specified at 565 kPa (82 psi), with a 7% turbulence intensity value. The turbulence intensity is scale which characterizes the turbulence expressed as a percent.  High speed flow inside complex geometries such as the IRV can be assumed to have high turbulence intensity level. The outlet was set as a mass flow outlet (negative mass flow inlet per CCM+) with mass flow rate = 5.674 kg/s. For the outlet boundary condition, a performance curve (see Fig. 5.9, [3]) was utilized to determine the approximate maximum flow rate through the IRV in a full by-pass situation using a set pressure of 565 kPa (82 psi). This procedure was used to form a direct linkage between set pressure and maximum flow through the pump. It is important to note that the performance curve is mainly used to describe pump performance, while

the maximum flow rate through the pump is influenced by pressure and viscosity. It was assumed in the current analysis that the maximum flow through the IRV in an over-pressure situation, where the IRV is subjected to full by-pass, is approximately equal to the maximum flow through the pump.

The default values in CCM+ were used to initialize the parameters:

- turbulence intensity: 1%

- pressure: 0 Pa

-turbulence viscosity scale = constant: 1.0 m/s

-turbulence viscosity ratio = constant: 10.0

-velocity: [0.0, 0.0, 0.0] m/s.

**Differential Pressure Performance Curve**

Max flow = 93.61GPM (5.674 kg/s)



**Calculated Values**
Input Flow: 191 GPM
Calculated Speed: 1470.78 RPM
Power at calc speed: 11.31 BHP

**Application Settings**
Model: KK124A
Viscosity: 32 SSU
Diff. Pressure: 82 PSI
Temperature: 20 C
Specific Gravity: 1

**Warnings**
Specified flow is greater than maximum-rated flow of 93.61 GPM

Viking Pump of Canada, A Unit of IDEX Corporation, 661 Grove
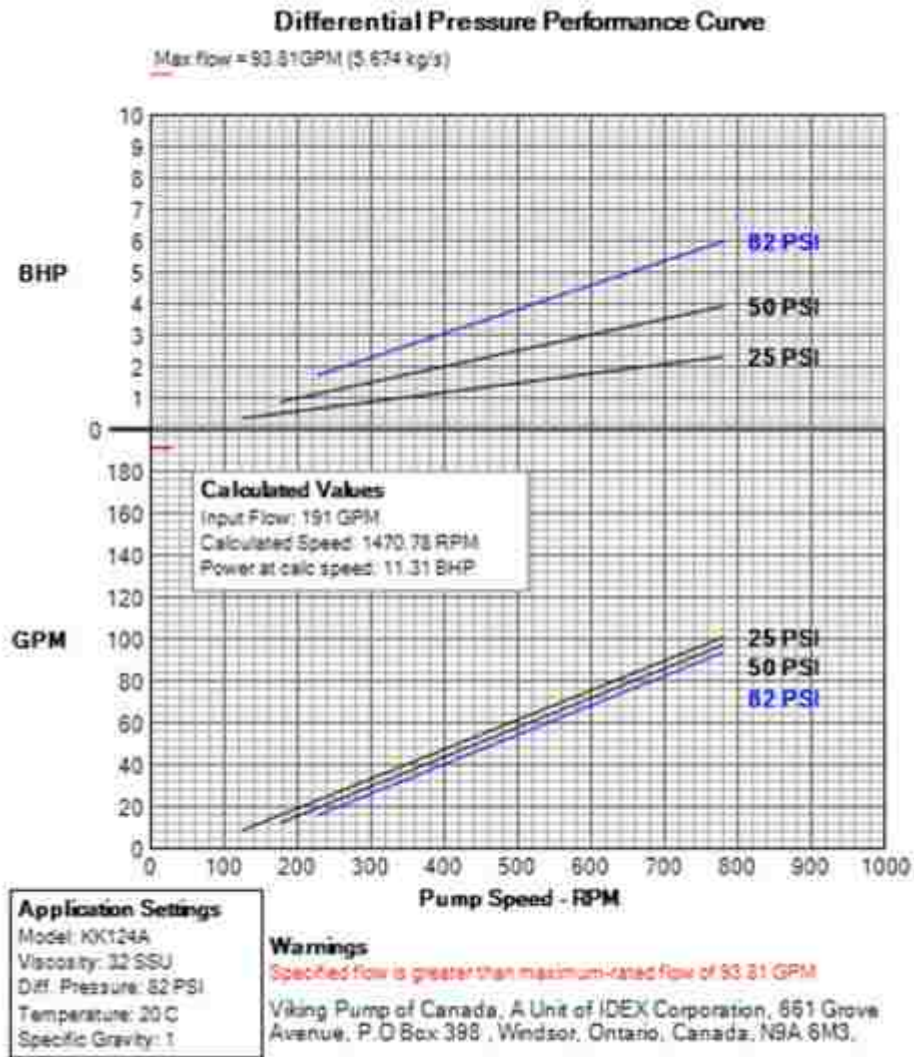Avenue, P.O Box 398 , Windsor, Ontario, Canada, N9A 6M3.

Fig. 5.9:  Performance curve - IRV set pressure setting = 565 kPa (82 psi) [8]

(by permission of Viking Pump Inc.)

All other components within the IRV such as the poppet, spring, bonnet, etc., as described above in Section 5.5, were set with wall boundary conditions. The opening gap (orifice width)/(offset distance) of the poppet was set to 0.64″.

The liquid flowing through the IRV is assumed to be incompressible and Newtonian (e.g., water). It is assumed that fluid temperature is ambient at a constant value of 20℃. It is also assumed that the problem is a steady flow problem with flow moving over static components in their fixed positions.

## 5.7.    IRV Simulations

Simulations were performed using both the standard $k$-$\varepsilon$ and $k$-$\omega$ turbulence models. Results from these simulations were compared to assess whether the $k$-$\varepsilon$ model, which is regarded as the industry workhorse, could accurately predict the flow parameters. However, the IRV geometry is complex and promotes flow separation as the liquid travels through it. The $k$-$\omega$ turbulence model was selected for subsequent analysis due to its ability to handle separated flows more effectively. First and second order upwinding for the convective terms were also investigated. Second order upwinding was used in further analysis to maintain more accuracy. The equation residuals as described earlier in chapter play an important role in assessing the accuracy of the solutions that were monitored. A stopping criterion of 6000 iterations was imposed, and all simulations converged well within this number of iterations.

The residuals shown in Fig. 5.10 and Fig. 5.11 are representative of the $k$-$\varepsilon$ and $k$-$\omega$ turbulence models using the $1^{st}$-order upwind scheme. All residuals have dropped below $1.0 \times 10^{-6}$. The continuity is of most importance and even though is it above other residuals, its residual drops below $1.0 \times 10^{-6}$ in less than 1000 iterations. Viewing these residuals, it is evident that the continuity residual fluctuates in a repetitive manner after a sufficient number of iterations, indicating that the solution is not changing significantly from one iteration to the next. The significance of having the solution run until 6000

iterations is to ensure nothing in solution has diverged after the solution has converged. This happens in the *k-ε* turbulence model at around 2000 iterations, while this behaviour can be observed with the *k-ω* model at around 1000 iterations.
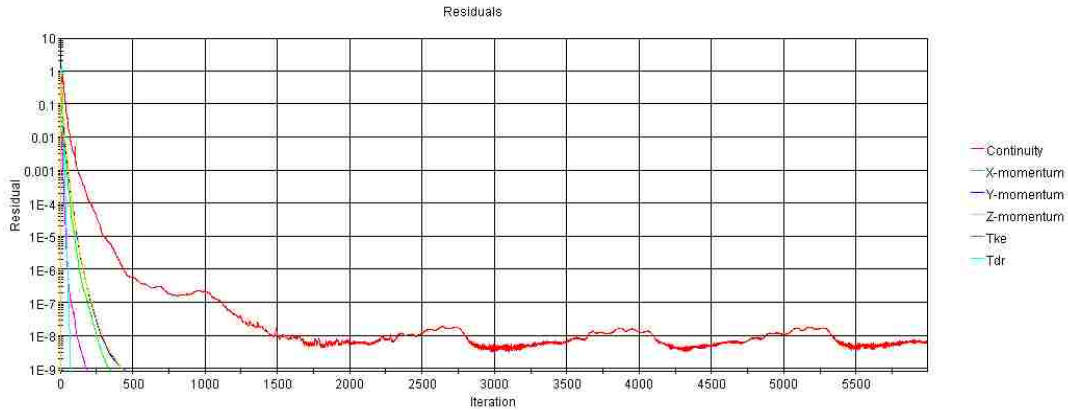


Fig. 5.10:  Residuals for *k-ε* turbulence model (1st-order upwind)
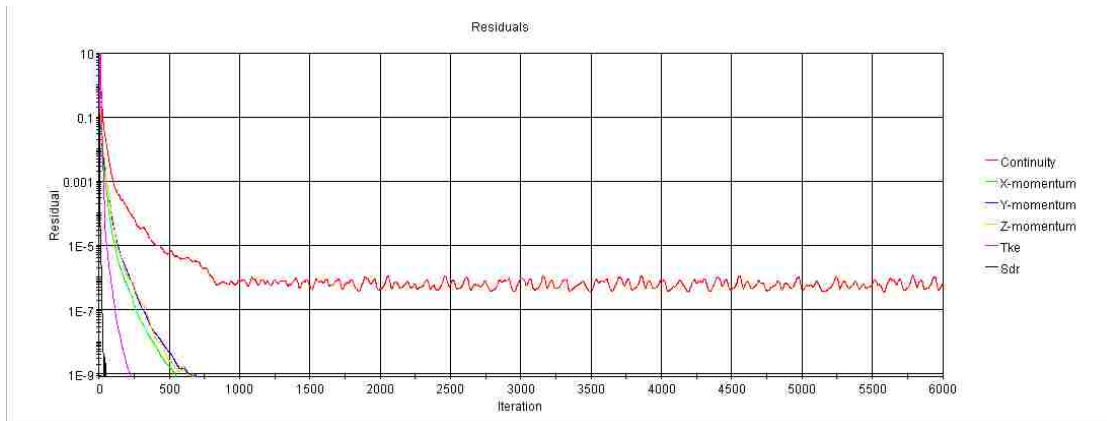


Fig. 5.11: Residuals for *k-ω* turbulence model (1st-order upwind)

The velocity vectors were also observed to get an idea of how the flow behaves within the valve. It is important to note that the velocity magnitude increases at the inlet and outlet ports. This is due to the fact that the diameter is not constant at the inlet and outlet ports. The IRV has assembly clearances within the design; this is to accommodate the attachment of the IRV to the pump using bolts as seen in Fig. 5.12. It should be noted

66

that the sole purpose of the clearance design is for installation. There were no flow considerations taken into account when the design was implemented.
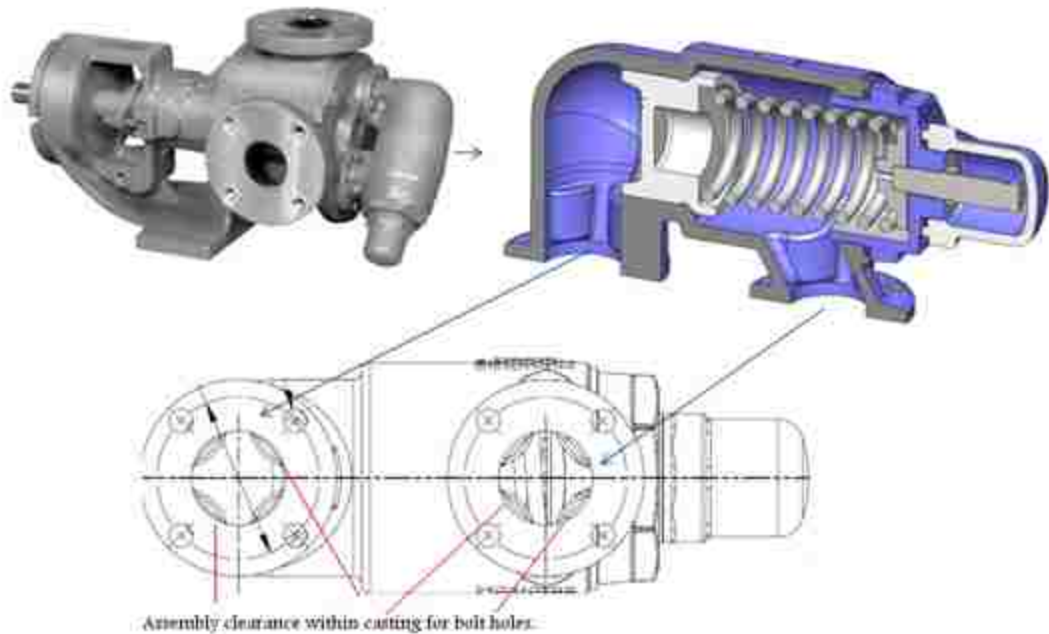


Fig. 5.12: IRV assembly clearance

The flow velocity increases through the gap where the poppet has an offset distance of 0.64″. Flow separation occurs at the sharper edges which induces flow recirculation. The velocity vectors also reveal the regions where the flow tends to reverse its direction due to the obstructions it encounters in the valve. The flow characteristics in the IRV (determined using CFD) help to identify how the flow can potentially be improved to increase the valve performance. These comments are reinforced in Figs. 5.13 and 5.14, illustrating the velocity vectors coloured by velocity magnitude based on the simulation using the first order upwind scheme. This cross-sectional view of the IRV illustrates how the flow physics operates within the IRV. Theoretically we would expect

to see the velocities in the IRV as shown in Figs. 5.13 and 5.14, based on the inlet and outlet boundary conditions used as stated above. In both the $k$-$\varepsilon$ and $k$-$\omega$ models, an accumulation of fluid tends to build up near the top left hand portion of the IRV. This accumulation of fluid is caused by the centrifugal effect of the flow near the top of poppet. This is mainly due to the fact that as the flow enters the valve it is not distributed evenly before encountering the poppet. The flow has taken the path of least resistance.
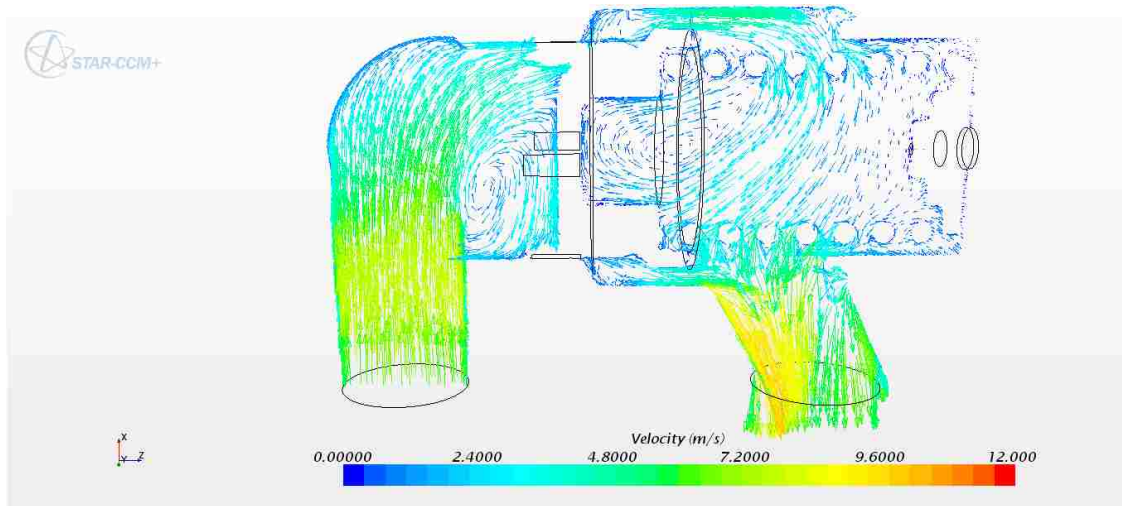


Fig. 5.13: Velocity vectors, coloured by velocity magnitude – $k$-$\varepsilon$ turbulence model; 1st-order upwind scheme
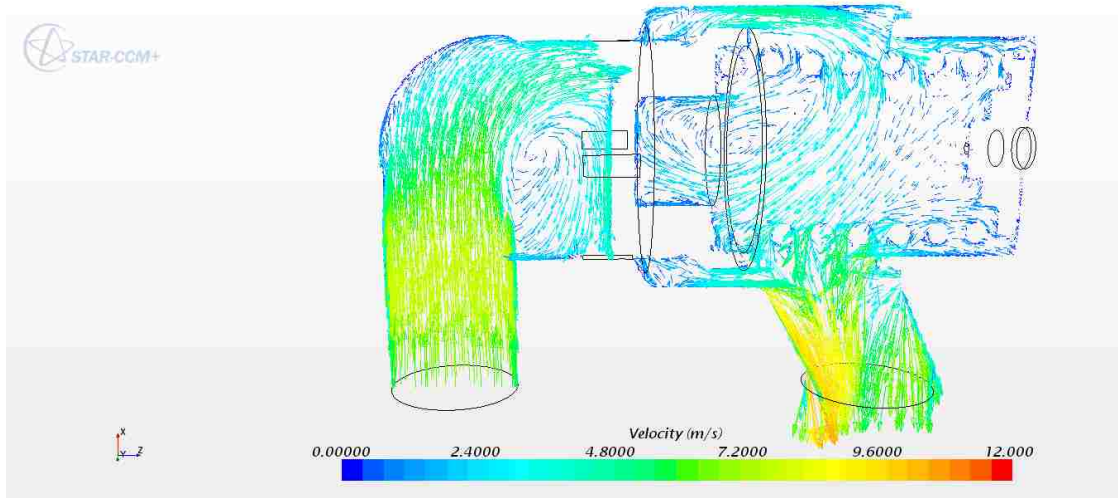
Fig. 5.14: Velocity vectors, coloured by velocity magnitude – $k$-$\omega$ turbulence model; 1$^{st}$-order upwind scheme

The 1$^{st}$-order upwind scheme was used in the preliminary stages because it tends to have better convergence properties than 2$^{nd}$-order schemes as a result of the added numerical diffusion associated with it. Results are obtained more quickly using the 1$^{st}$-order scheme, which is especially beneficial when performing sensitivity analyses with the simulations. The various numerical parameter settings noted above were determined after extensive tests with different parameters such as the mesh size, number of prism layers, relaxation factors, etc., all of which contribute to the sensitivity analysis. To increase the accuracy of the solution, the maximum number of iterations and the upwind scheme can be changed. It was decided to keep the maximum number of iterations set at 6000 since the 1$^{st}$-order upwind scheme yielded good results with much less than this number of iterations. Therefore, the only change implemented was changing from a 1$^{st}$-order to a 2$^{nd}$-order upwind scheme. All other physical and numerical parameters were kept the same as stated above.

Figures 5.15 and 5.16 illustrate the residuals from the 2$^{nd}$-order simulations for the $k$-$\varepsilon$ and $k$-$\omega$ turbulence models. The residuals for all the fluid dynamics equations except continuity drop below $1.0 \times 10^{-8}$ within 1000 iterations. The continuity residual for the $k$-$\varepsilon$ turbulence model drops slightly below $1.0 \times 10^{-7}$ at 2000 iterations before it starts to stabilize. The continuity residual for the $k$-$\omega$ turbulence model drops to $1.0 \times 10^{-5}$ at 500 iterations and then levels out slightly about this value in subsequent iterations.
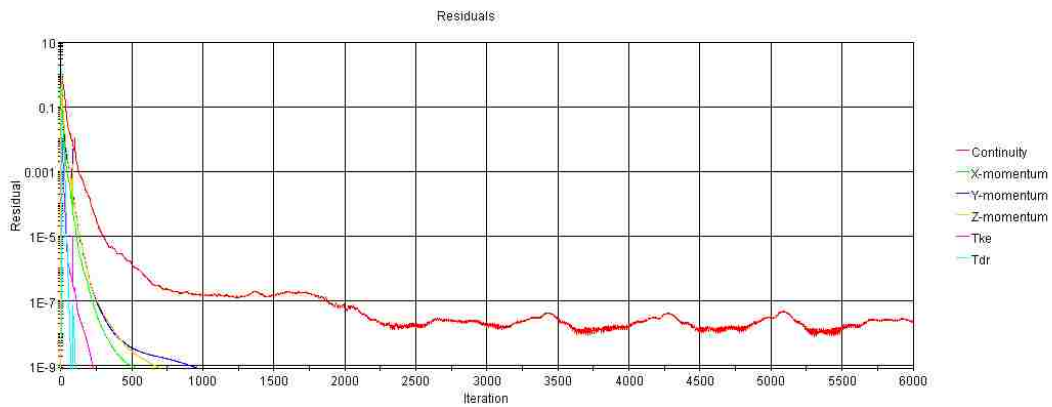


Fig. 5.15: Residuals for $k$-$\varepsilon$ turbulence model (2$^{nd}$-order upwind)
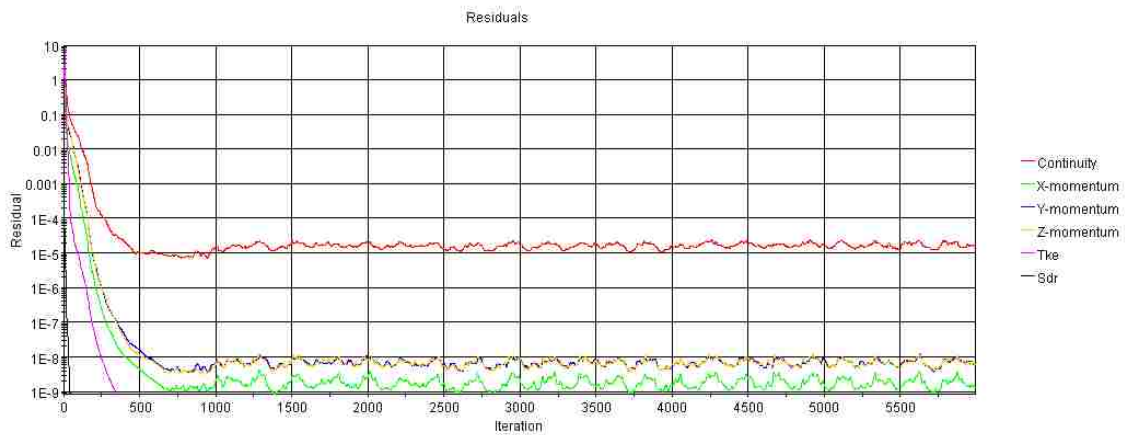


Fig. 5.16: Residuals for $k$-$\omega$ turbulence model (2$^{nd}$-order upwind)

The differences between the $k$-$\varepsilon$ and $k$-$\omega$ turbulence models are quite evident. The $k$-$\omega$ model appears to stabilize much sooner, after about 500 iterations, while the $k$-$\varepsilon$

model requires about 2500 iterations to reach a stable value. Since the flow in the IRV is complicated, with separation and large recirculation regions, it was decided that the $k$-$\omega$ turbulence model would be best in capturing the flow field within the IRV.

The velocity vectors are shown in Fig. 5.17, coloured with velocity magnitude. The $k$-$\omega$ model turbulent model with a $2^{nd}$-order upwind scheme is used. The predicted flow field appears to be more realistic than that obtained with the $1^{st}$-order scheme. Flow separation and recirculation is captured, along with the flow reaction to discontinuities within the IRV. The change in direction of the velocity vectors illustrates the reversal of the flow at the inlet section and when the flow goes around the spring and other cavities in the outlet section of the IRV.
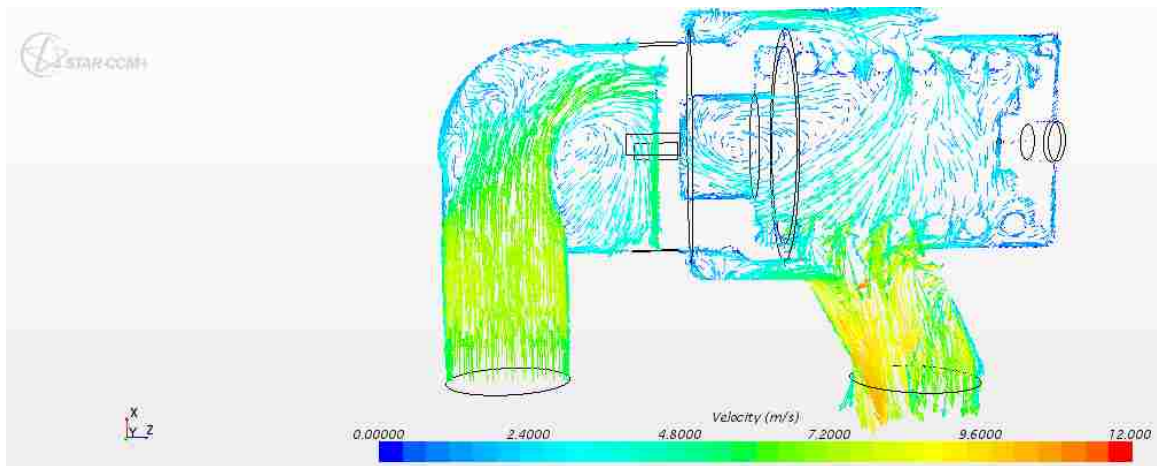


Fig. 5.17: Velocity vectors, coloured by velocity magnitude – $k$-$\omega$ turbulence model; $2^{nd}$-order upwind scheme

The contours of velocity magnitude are shown in a cross-section of the IRV when viewing from the top of the IRV in Fig. 5.18. The cross section is taken from the top of the IRV. The flow accelerates in smaller areas where the vena contracta (orifice) exist. The offset region where the poppet is pushed back is where the increase in velocity

71

occurs. The velocity also increases at the entrance and exit of the IRV due to the assembly clearance for the bolt holes. The velocity magnitude superimposed with 3D streamlines is also plotted in the xz plane. The main purpose of plotting the streamlines is to observe the flow pattern as the fluid moves from the inlet port of the IRV to the outlet port. When viewing the streamlines in Fig. 5.19, the chaotic flow behaviour in the IRV is quite evident.
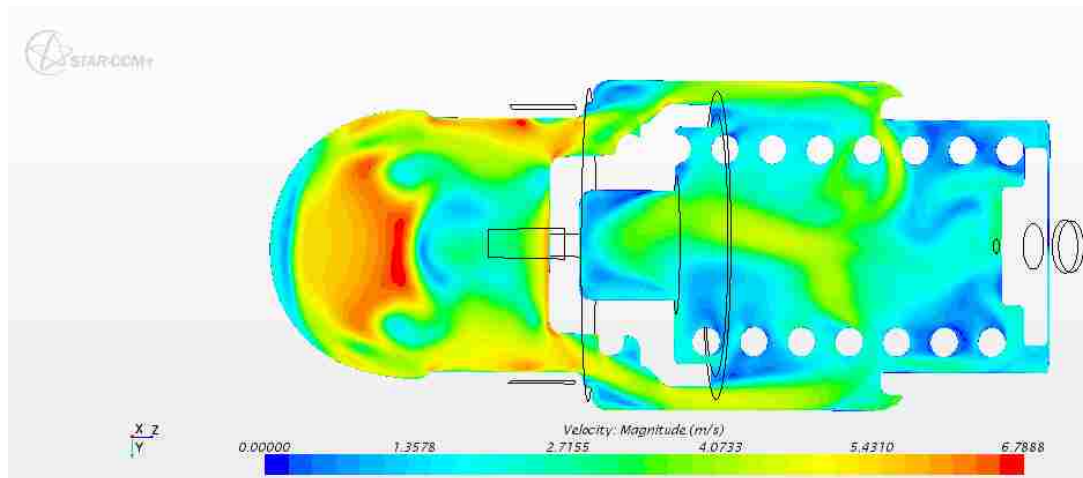


Fig. 5.18: Velocity magnitude contours – $k$-$\omega$ turbulence model; $2^{nd}$-order upwind
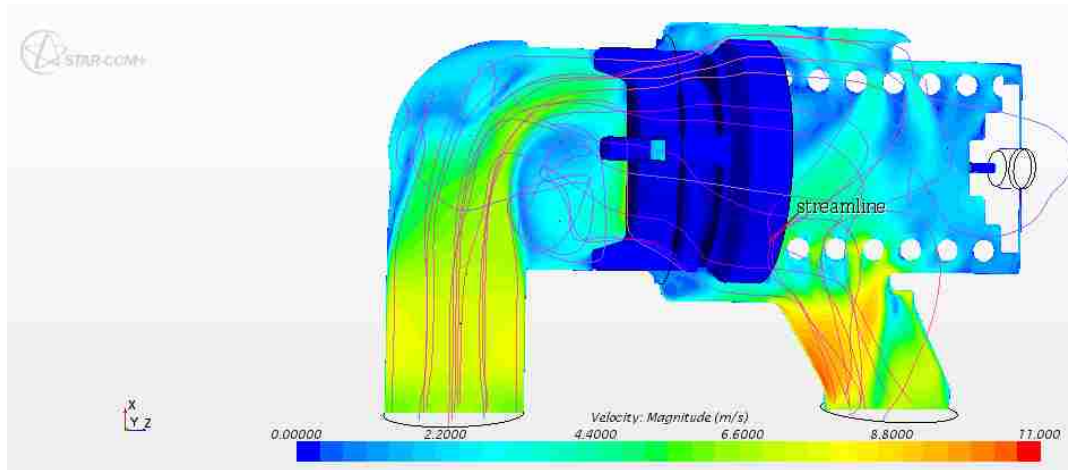
scheme

Fig. 5.19: Velocity magnitude contours and streamlines – $k$-$\omega$ turbulence model;

2nd-order upwind scheme

The total pressure is of primary importance. The IRV setting is solely dependent on the set pressure in reference to which spring range is used in the IRV. The pressure contours in Fig. 5.20 illustrate that the assembly clearance for the bolt holes does increase the pressure at the inlet of the IRV. The pressure should also be higher on the inlet side of the IRV due to restriction caused by the poppet, which the contours confirm. The contours in Fig. 5.20 also help to understand the relationship between pressure and the valve offset distance. It can be seen that irrespective of the valve offset distance there will always be greater pressure on the inlet side of the IRV due to the placement of the poppet in the valve, which acts as a restriction within the IRV.
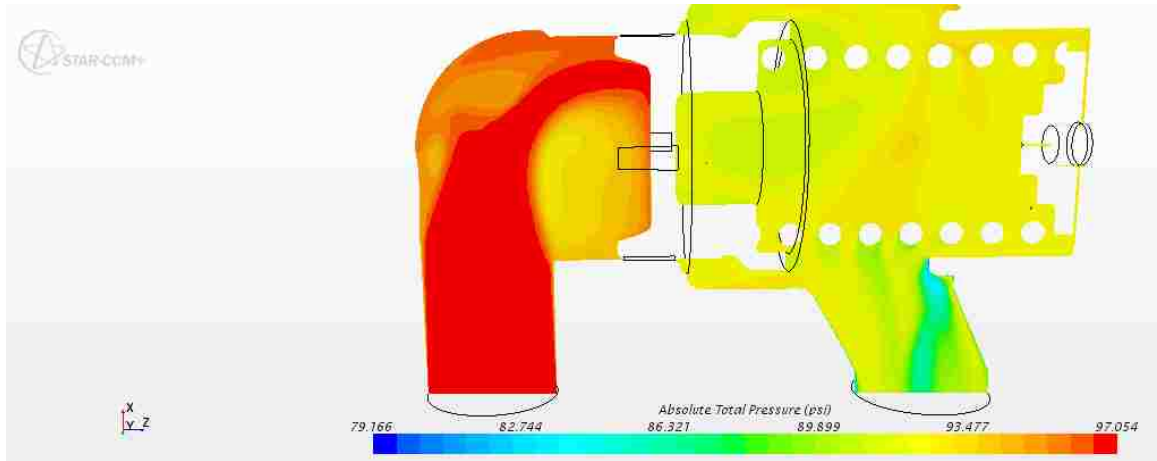
Fig. 5.20: Total absolute pressure – $k$-$\omega$ turbulence model; $2^{nd}$-order upwind scheme

Observing the wall Y+ values on the IRV shell, as demonstrated in Fig. 5.21, the range is approximately from 15 to 20. When viewing the cross-section shown in Fig. 5.22, the Y+ values are approximately from 4 to 9. Based on the standard meshing and prism layer meshing applied, these wall Y+ values allow the simulations to capture the flow characteristics at the wall. In earlier trial simulations, divergence occurred quite frequently before the prism layer mesh was implemented. With the prism layer mesh implemented, the divergence issue was corrected and convergence realized.
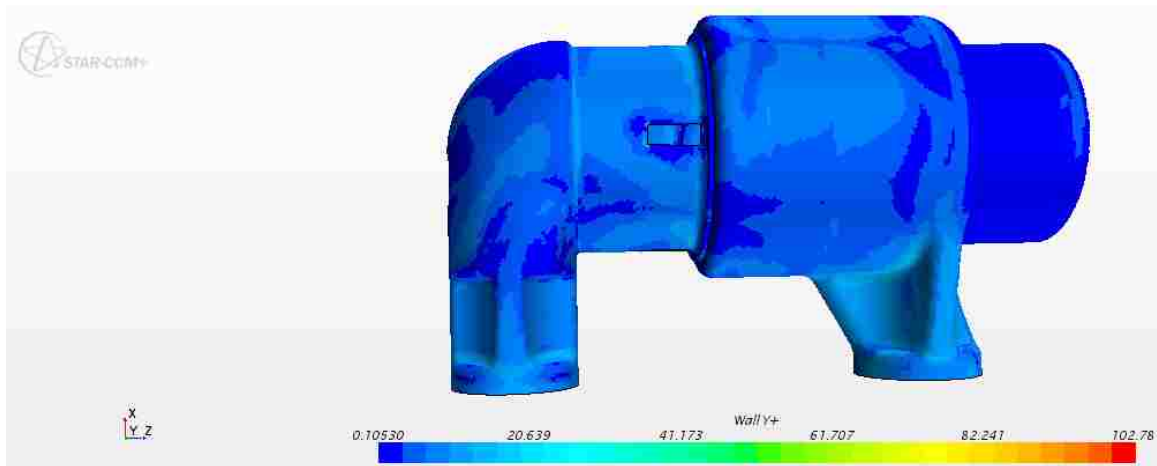


Fig. 5.21: Wall Y+ of IRV shell –$k$-$\omega$ turbulence model; $2^{nd}$-order upwind scheme

74
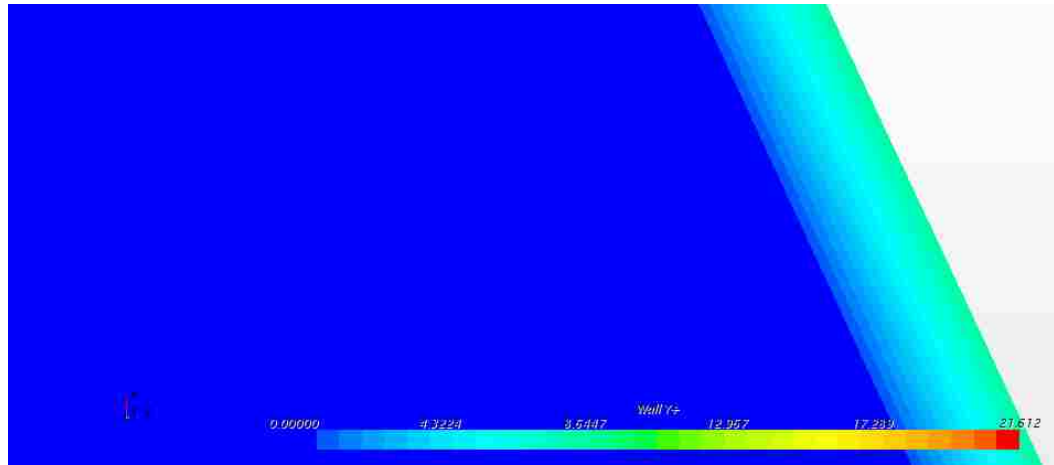
Fig. 5.22: Wall Y+ of IRV cross-section (near-wall)

# CHAPTER 6.   CONCLUSIONS AND RECOMMENDATIONS

## 6.1.      Conclusions

The external valve and internal relief valve were both studied and analysed. Conclusions have been drawn from the findings.

*External Relief Valve (ERV)*

The objective of the ERV simulations was to test several key factors that are known to affect the successful implementation of commercial CFD software. Chapter 4 concentrated on developing a simplified model of the ERV that could be used to perform numerical sensitivity analyses with respect to several physical and computational parameters, thereby acquiring valuable knowledge. The 2D ERV simulations provided guidance in deciding which parameter settings were best to use for the 3D ERV analysis, and subsequently for the internal relief valve (IRV) study. The work done on the ERV helped identify key areas that require special attention, such as appropriate mesh size and characteristics, when to use a fine/coarse mesh, location and implementation of boundary conditions, turbulence modeling, etc. Numerical tests involving adjustments to parameters such as convergence criteria, relaxation factors, upwind schemes and selection of a solver helped capture more accurate solutions.

The 2D ERV model underwent many improvements which subsequently helped with the 3D analysis of the ERV. Certain criteria were checked at the 2D stage to ensure that the model correctly predicted the flow physics. Preliminary simulations indicated significant back flow re-entering the outlet port of the ERV. This was resolved by extending the outlet nozzle. Plots of the velocity vectors in the extended outlet were used

to determine the length of the outlet nozzle needed to eliminate back flow at the outlet. It was also concluded that the inlet nozzle should be extended inside the valve body to form a curtain, thereby creating a converging/diverging flow which is more representative of the actual relief valve configuration. The 3D ERV model was based on the changes made in the 2D stage. Major changes discussed above were the specific aspects implemented in the 3D model.

*Internal Relief Valve (IRV)*

The analysis performed on the 2D and 3D ERV models provided valuable input to initiate the setup for the IRV simulation. Manipulation of some of the numerical parameters such as the meshing/prism layers, relaxation factors and choice of solver helped to promote convergence in the simulation. It can also be concluded that there was a significant difference in the predictions from the $k$-$\varepsilon$ and $k$-$\omega$ turbulence models. The $k$-$\omega$ model captured the flow reversal and recirculation within the IRV more accurately. From the simulation results it was seen that the IRV has some structural features that do not promote desired flow characteristics within the IRV. Based on the IRV simulations, it appears that there are some areas where potential improvements could be made to enhance the performance of the IRV by reducing the pressure range from cracking to full by-pass pressure. The recommendations below further show how the desired outcome is potentially realized.

## 6.2. Recommendations

*IRV – General Recommendation*

The main objective of this thesis was to provide some scientific and engineering guidance with respect to improving the IRV performance. The ultimate goal is to reduce pressure range from the cracking to full by-pass. Viewing the flow dynamics and the behaviour of the fluid within the IRV has helped to identify some areas where improvement could be made. For future work once a sound design is approved through experimental validation the web based curve generator located on the Viking Pump Inc. website would be modified to incorporate changes related to improved IRV performance.

The IRV flow vectors shown in Fig. 5.17 suggest that the flow entering the IRV from the inlet is not uniformly distributed when it impinges on the poppet, which creates a larger force on one side of the poppet. It is assumed in this case that the poppet is at its fully open position, it cannot be confirmed at this time if when poppet is ½ open if this uniformity still exists. Since the force of the fluid is not uniformly distributed along the face of the poppet, this can cause a potential torque applied to the poppet with one side of the poppet and spring tending to rotate as illustrated in Fig. 6.1. However, it is desirable to keep the poppet moving in the axial direction as it moves back and forth. During poppet chatter this may be one of the causes for the poppet becoming unseated when it is returned back to its closed state. By improving the flow distribution the cracking to full by-pass pressure should be reduced. There would be a more uniform force distribution applied to the entire poppet face rather than a larger force at the top of the poppet.

Fluid Force is near the top of the poppet. The majority of the fluid force contacts this region

This causes poppet to rotate instead of maintaining its linear movement back and forth

Velocity (m/s)

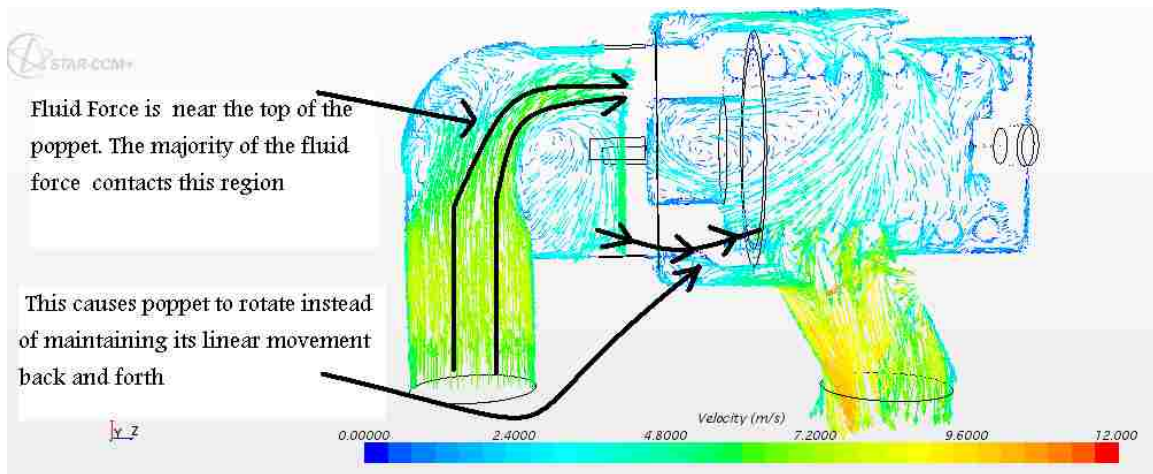Fig. 6.1: Illustration of flow interaction with the poppet

*IRV – Recommendation #1*

To create a more uniformly distributed flow, vanes at the inlet elbow can be implemented as shown in Fig. 6.2. Rounding out the sharp 90° bend at the bottom of the valve would also help to achieve better flow distribution and reduce the flow separation, thereby reducing the size and strength of the flow recirculation region.
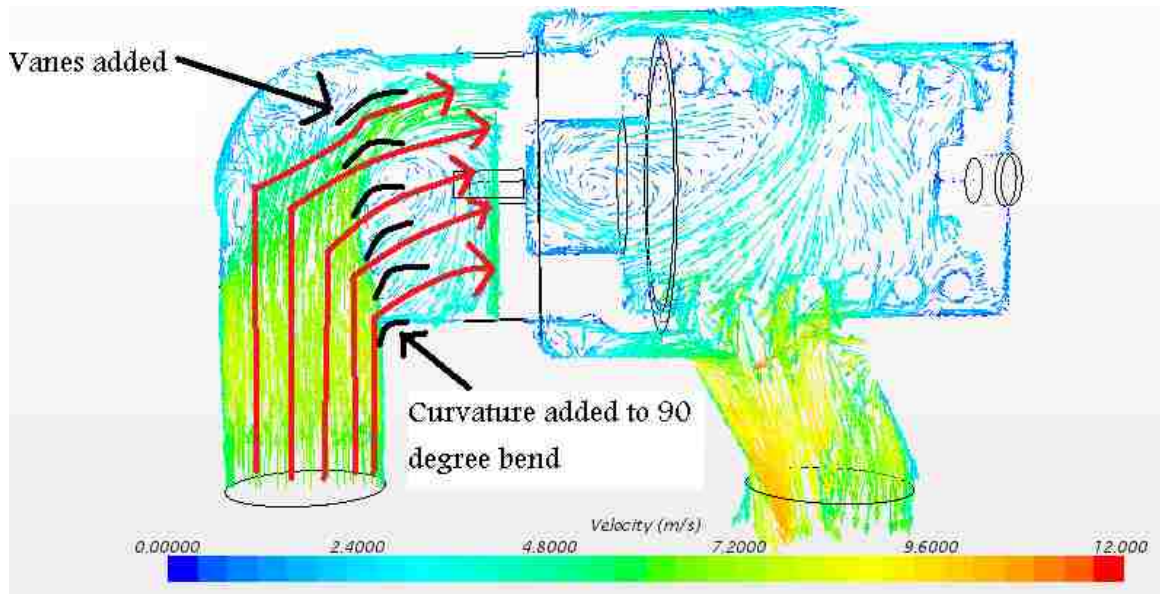
Fig. 6.2: Added features for better flow distribution

*IRV – Recommendation #2*

The ERV operates with the converging-diverging nozzle principle. The simulations in Chapter 4 where the converging diverging nozzle principle was elaborated on indicate that increasing the size of the nozzle after the throat produces an expansion which results in a pressure drop. The same principle is applied to the IRV. By increasing the diameter of the IRV body, the clearance after the throat would be enlarged to yield the same benefits. Creating more expansion after the orifice (gap between the valve seat and poppet) will also yield a wider range of pressure drop. With more pressure the cracking to full by-pass would be reduced as well as illustrated in Fig 6.3. Another change that would enhance the effect of the converging/diverging principle would be to remove the assembly clearances for the bolt holes. This would ensure that the areas at the inlet and outlet ports are much larger than the throat area in the IRV where the poppet is positioned.
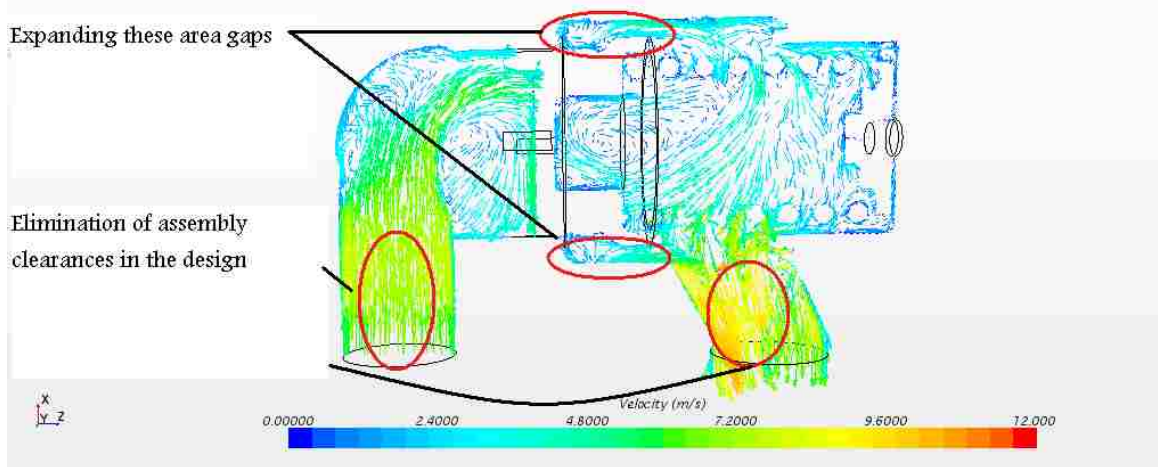
Fig. 6.3: Removal of assembly clearance and wall thickness

*IRV – Recommendation #3*

Another potential improvement would result from the removal of the guide vanes and increasing the poppet diameter to contact the internal wall of the IRV while maintaining the same clearance as the guide vanes, as shown in Fig. 6.4. The assembly clearances would also be removed. The idea behind this concept is to reduce the losses at the front face of the poppet. Since the losses would be reduced, the time from cracking to full by-pass pressure would be decreased due to maximizing the flow through the valve.
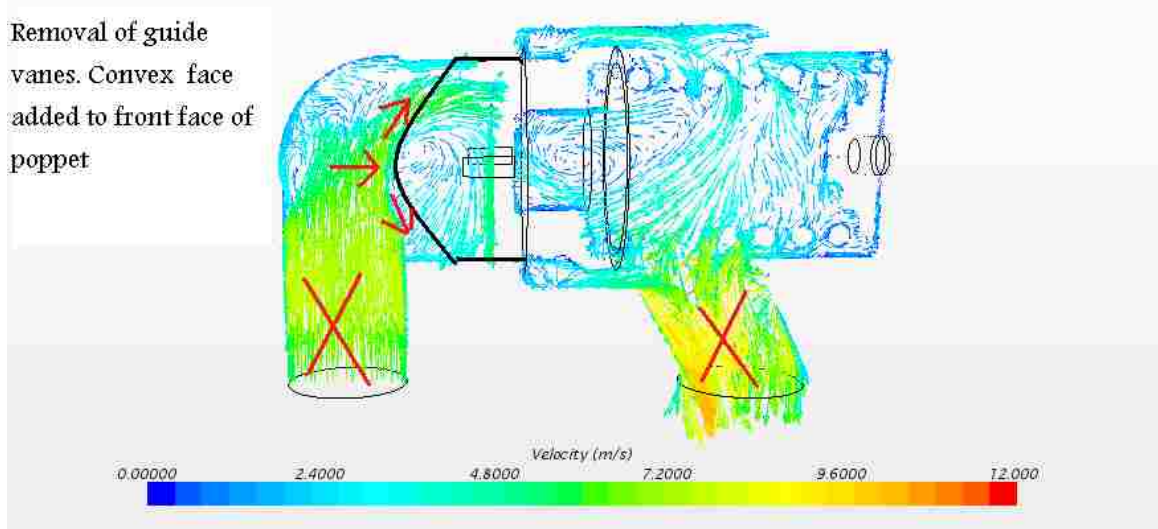
Fig. 6.4: Adding convex curvature to front face of poppet and removal of guide vanes

These recommendations are based on results obtained from the sensitivity analyses and careful examination and interpretation of the velocity and pressure fields in the IRV. It can be concluded that the valve has many features which were not designed with the intent to accommodate how the flow would react inside the IRV. The main motivation behind the recommendations is to improve the cracking to full by-pass pressure. This would be beneficial in achieving a well-designed IRV which would be more competitive in the oil and gas industry, while maintaining its technical function for safety.

# REFERENCES

[1]     Mayer, J. Viking Standard Relief Valve Performance Modelling. W.O. 4592, Viking Pump Inc., Iowa, 1984.

[2]     Kourakos, V., Rambaud, P., Chabane, S. Flow Force in a Safety Relief Valve Under Incompressible, Compressible and Two Phase Flow Conditions. *Journal of Pressure Vessel Technology*, Vol 135, pp. 1-11, 2013.

[3]     Chabane, S., Plumejault, S., Pierrat, D., Couzinet, A., Bayart, M. Vibration and Chatterring of Conventional Safety Relief Valve Under Built Up Back Pressure. *3rd IAHR International Meeting of the Work Group on Cavitation and Dynamic Problems in Hydraulic Machinery and Systems*, Brno, Czech Republic, 2009.

[4]     Follmer, B., Schnettler, A. Challenges In Designing API Safety Relief Valve. *Valve World*, 10, pp. 39-43, 2003.

[5]     Bilanin, A.J., Teske, M.E. Modelling Flow Through Spring-loaded Safety Valves. *PVP: Journal*, Vol 190, pp. 29-36, 1990.

[6]     Oravec, J. A Steady State Approach to Calculation of Valve Pressure Rise Rate Characteristics. *Konference Paper Ansys*, 2011.

[7]     Sethi, S., Lai, Y.S. A Simulation Model to Predict the Performance Characteristics of Safety Relief Valves. *Proceedings of Sum Computer Simulation Conference (SCSC'93)*, pp. 800-806, 1993.

[8]     Viking Pump Inc. http://www.vikingpump.com/, 2014.

[9]     Viking Pump Inc. Technical Service Manual, Section TSM000, Issue H, pg.1-8, 2009.

[10]    Helleman, M. *Safety Relief Valve Handbook. Design and Use of Process Safety Valves to ASME and International Codes and Standards*. pp. 79-109, Elsevier Ltd, Burlington, MA, 2009.

[11]    Viking Pump Inc. Service Bulletin ESB 31, pp. 1-4, 1985.

# BIBLIOGRAPHY

[1]     Malek, M. *Pressure Relief Devices:ASME and API Code Simplified.* McGraw-Hill Inc, New York, 2006.

[2]     Westaway, C.R., Loomis, A.W. *Cameron Hydraulic Data*. Sixteenth Edition, Ingersoll-Rand Company, Woodcliff Lake, N.J., 1979.

[3]     Hoffmann, K.A., Chiang, S.T., Computational Fluid Dynamics, Vol III, Fourth Edition, Engineering Education System, Wichita, KS, USA, 2000.

[4]     Engineering Division. Flow of Fluids Through Valves, Fittings and Pipes. Technical Paper No 410-C, Crane Co. Canada Ltd, 1969.

[5]     Streeter, V. *Fluid Dynamics.* McGraw-Hill Inc., New York, Toronto, London, 1948.

[6]     Streeter, V. *Handbook of Fluid Dynamics*. First Edition, McGraw-Hill Inc., USA, 1961.

[7]     Streeter, V., Wylie, B. *Fluid Mechanics*. Eight Edition, McGraw-Hill Inc., USA, 1986.

[8]     Chabane, S., Kourakos, V., Rambaud, P., Buchlin, J. Hydrodynamic Forces, Pressure and Mass Flux in Two-phase Air-water Flow through Transparent Safety Valve Model. *ASME 2010 Pressure Vessels and Piping Conference*, Bellevue, WA, American Society of Mechanical Engineers Paper No. PVP2010-25440, pp. 1-8, 2010.

[9]     Liptak, B. *Instrument Engineers Handbook, Volume I: Process Measurement*. Chilton Book Company, Philadelphia, New York, London, 1969.

[10]   Liptak, B. *Instrument Engineers Handbook, Volume II: Process Measurement.* Chilton Book Company, Philadelphia, New York, London 1970.

[11]   McCabe, W., Smith, J., Harriott, P. *Unit Operations of Chemical Engineering.* Fourth Edition, McGraw-Hill Inc, USA, 1985.

[12]   Smith, P., Zappe, R.W. *Valve Selection Handbook. Engineering Fundamentals for Selecting the Right Valve Design for Every Industrial Flow Application.* Elsevier Ltd, Burlington, MA, 2004.

# APPENDICES

## APPENDIX A - Copyright Permission Documents

**From:** Nantau, Chris

**Sent:** Thursday, July 24, 2014 8:48 AM

**To:** Henry, Yohance; Goddard, Derrick; Toy, Joe

**Cc:** Yohance Henry (henry8@uwindsor.ca)

**Subject:** RE: Pictures of Actual Relief Valve (THESIS)-Yohance


No problem Yohance. Our only concern would be if you used actual component

drawings showing sensitive information, dimensions etc. This is not the case so go ahead

and good luck.


*Chris Nantau – Director of Sales, – Canada and European Operations*

*Viking Pump and Wright Flow – Units of IDEX Corporation*


661 Grove Avenue, Windsor, Ontario  N9A 6M3

E-Mail:  **cnantau@idexcorp.com** | **Web: www.vikingpumpcanada.com**; **www.wrightflowtechnologies.com**

**Office:**  888-845-7867  ext: 4296| **Mobile:**  519-259-2715 | Fax: 888-803-8640




VIKINGPUMP.COM | SANDPIPERPUMP.COM | WRIGHTFLOWTECHNOLOGIES.COM
CONTACT US TODAY TO LEARN HOW KITS WILL SAVE YOU TIME AND MONEY

**From:** Henry, Yohance

**Sent:** Thursday, July 24, 2014 8:37 AM

**To:** Goddard, Derrick; Nantau, Chris; Toy, Joe

**Cc:** Yohance Henry (henry8@uwindsor.ca)

**Subject:** Pictures of Actual Relief Valve (THESIS)-Yohance

Good Morning Derrick, Chris and Joe,

The pictures below represent the actual physical relief valve in real life. I will be

performing the CFD simulations on the 3-dimensional (3D) RV data which represents the

physical relief valve in the pictures below. This is the same 3D data I had shown to all of

you in my last presentation.  I would like to have permission to include these pictures in

my Thesis write up/presentation. I would like to include some practical components in

my thesis as well. Please let me know if this is okay.

Thanks again for the support.

**Yohance Henry, M.Eng., P.Eng.  -** *Application Engineer*

**Viking Pump of Canada** –  A Unit of IDEX Corporation

661 Grove Avenue, Windsor, Ontario  N9A 6M3

**E-Mail**:**yhenry**@idexcorp.com | **Web:** **www.vikingpumpcanada.com**

**Office:**  519-259-4268 | **Fax:**  519-256-5070

Figure A.1 – Permission for use of Viking Pump Inc. relief valve in thesis

-----Original Message-----
From: Goddard, Derrick
Sent: Tuesday, April 07, 2015 6:25 PM
To: Henry, Yohance
Cc: Toy, Joe; Yohance Henry (henry8@uwindsor.ca)
Subject: Re: Additional Figures included in THESIS-Yohance

Approved

Sent from my iPhone

On Apr 7, 2015, at 5:57 PM, Henry, Yohance<YHenry@idexcorp.com> wrote:

Good afternoon Derrick,

 As a standard protocol I must ask to have permission to include the list of figures into my final Thesis. None of the figures contain dimensions of any sort/proprietary  information.

 Can you please review and let me know if you have any concerns/reservations. I 've attached the word document for your reference.


 Thanks and best Regards.

Yohance Henry, M.Eng.,P.Eng.  - Application Engineer
 Viking Pump of  Canada –  A Unit of IDEX Corporation
 661 Grove Avenue, Windsor, Ontario  N9A 6M3
 E-Mail:  yhenry@idexcorp.com<mailto:yhenry@idexcorp.com>|  Web: www.vikingpumpcanada.com<http://www.vikingpumpcanada.com/>
 Office:  519-259-4268 | Fax:  519-256-5070
 [cid:image002.jpg@01CFBAD1.28E967B0]


Figure A.2 – Permission for use of Viking Pump figures in thesis [8], [9], [11]

Dear Prof. Henry,

I apologize, the copy I had must have been cut off.  I have revised the permission letter to include Figure 13.  It is our pleasure to grant you permission to publish the ASME **Figures 1, 2, 4,6,13 and Table 1** from "Flowforce in Safety Relief Valve Under Incompressible, Compressible and Two-Phase Flow Conditions," by Vasilios Kourakos, Saïd Chabane, Patrick Rambaud and Jean-Marie Buchlin, Paper No. PVP2011-57896, as cited in your letter for inclusion in a journal/magazine entitled Improved Internal Relief Valve Performance Study Of Reduced Cracking To Full By-Pass Pressure Using CFD Simulation to be published by University of Windsor, Ontario, Canada.

Permission is granted for the specific use as stated herein and does not permit further use of the materials without proper authorization.  Proper attribution must be made to the author(s) of the materials.  As is customary, we request that you ensure proper acknowledgment of the exact sources of this material, the authors, and ASME as original publisher. Acknowledgment must be retained on all pages printed and distributed.

In accordance with ASME policy, this permission is contingent upon payment of a **royalty fee of US$50 for 6 figures** (at a discounted price). This is solely charged to non-authors of the requested ASME papers. We accept payments on all major credit cards such as: Visa, MasterCard, American Express, Discover, and Diners Club, or by check payable to ASME.  Please send payment to the attention of the Accounts Receivable Department, ASME, 22 Law Drive, Fairfield, NJ 07007, and indicate that this is a permission payment.  Should you have any questions regarding payment form or transfer, please contact AccountsReceivable@asme.org.

ASME does not hold the copyright of the following figures:

• Figure 3a original source of this figure is referenced in the paper by Chabane, S., Plumejault, S., Pierrat, D., Couzinet, A., and Bayart, M., 2009. "Vibration and chattering of conventional safety relief valve under built up back pressure". In 3rd IAHR International Meeting of the WorkGroup on Cavitation and Dynamic Problems in Hydraulic Machinery and Systems, International Association of Hydro-Environment Engineering and Research,

• Figure 3b original source of this figure is referenced in the paper by Corbin, F., Pozzoli, R., and Francois, P., 2009. Essais de soupapes-Banc eau. Documents Qualite CETIM T-8600-a, Centre Technique des Industries Mecaniques, Techniques des fluides et des ecoulements, 74 route de la Joneliere BP 82617, 44326 Nantes Cedex 3.

Unfortunately, ASME cannot grant permission for usage of Figures 3a and 3b.  Please

contact the original source for permission.

Many thanks for your interest in ASME publications.

Sincerely,

**Beth Darchi**

Publishing Administrator

ASME

2 Park Avenue, 6th Floor

New York, NY 10016-5990

Tel  1.212.591.7700

darchib@asme.org

Figure A.3 – Permission for use of figures 1, 2, 4 and 6 in reference [2]

Note: Copyright.com supplies permissions but not the copyrighted content itself.

CONFIRMATION

## Step 3: Order Confirmation

Thank you for your order! A confirmation for your order will be sent to your account email address. If you have questions about your order, you can call us at +1.855.239.3415 Toll Free, M-F between 3:00 AM and 6:00 PM (Eastern), or write to us at info@copyright.com. This is not an invoice.

**Confirmation Number: 11347867**
**Order Date: 04/26/2015**

If you paid by credit card, your order will be finalized and your card will be charged within 24 hours. If you choose to be invoiced, you can change or cancel your order until the invoice is generated.

### Payment Information

You are already
rakan.t@yahoo.com
+1 (519) 915-2214
Payment Method: n/a

### Order Details

| | |
|---|---|
| Order detail ID: 66846877 | Permission Status: Granted |
| Order License Id: 3616581472416 | Permission type: Republish or display content |
| ISBN: 978-1-85617-712-2 | Type of use: Thesis/Dissertation |
| Publication Type: Book | |
| Publisher: Butterworth-Heinemann | |
| Author/Editor: Hellemans, Marc | |

| | |
|---|---|
| Requestor type | Academic institution |
| Format | Print, Electronic |
| Portion | chart/graph/table/figure |
| Number of charts/graphs/tables/figures | 1 |
| Title or numeric reference of the portion(s) | Figure 5.10 - General design of spring operated SRV. I have edited this figure in my Thesis by showing the flow pattern with arrow identifiers and circled this area. This was done to illustrate the control volume that would be modelled in my CFD simulation |
| Title of the article or chapter the portion is from | Chapter 5: Design Fundamentals |
| Editor of portion(s) | Marc Hellemans |

Figure A.4 – Permission for use of one figure on page 85 in reference [10]

93

Throat → Curtain area = π x D x H = π x 76.2mm x 76.2 mm = π5806.44 mm$^2$

Inlet area = (π x D$^2$)/4 =  π1451.61 mm$^2$

Outlet area = (π x D$^2$)/4 =  π1451.61 mm$^2$

NOTE: Inlet and Outlet area are smaller than throat area.

Figure B.1 – Divergent-convergent model (3D), incorrectly depicting an ERV

Throat → Curtain area = π x D x H = π x 76.2mm x 12.7mm = π967.74 mm$^2$

Inlet area = (π x D$^2$)/4 =  π1451.61 mm$^2$

Outlet area = (π x D$^2$)/4 =  π1451.61 mm$^2$

NOTE: Inlet and Outlet area are now larger than throat area.

Figure B.2 – Convergent-divergent nozzle (3D), correctly depicting a valve

analogous to an ERV

# VITA AUCTORIS

NAME:                    Yohance Bakari Henry

PLACE OF BIRTH:          Windsor, ON


YEAR OF BIRTH:           1981


EDUCATION:               St. Joseph  High School, Windsor, ON, 2000

                         University of Windsor, B.A.Sc.,  Windsor, ON, 2004

                         University of Windsor, M.Eng., Windsor, ON, 2009

                         Professional Engineers Ontario, P.Eng.

                         Windsor, ON, 2010